Friction **10**(8): 1137–1165 (2022)
https://doi.org/10.1007/s40544-021-0586-1
ISSN 2223-7690
CN 10-1237/TH

REVIEW ARTICLE

Unlocking the secrets behind liquid superlubricity: A state-of-the-art review on phenomena and mechanisms

Tianyi HAN, Shuowen ZHANG, Chenhui ZHANG*
State Key Laboratory of Tribology, Tsinghua University, Beijing 100084, China
Received: 05 September 2021 / Revised: 29 October 2021 / Accepted: 08 December 2021

Abstract: Superlubricity, the state of ultralow friction between two sliding surfaces, has become a frontier subject in tribology. Here, a state-of-the-art review of the phenomena and mechanisms of liquid superlubricity are presented based on our ten-year research, to unlock the secrets behind liquid superlubricity, a major approach to achieve superlubricity. An overview of the discovery of liquid superlubricity materials is presented from five different categories, including water and acid-based solutions, hydrated materials, ionic liquids (ILs), two-dimensional (2D) materials as lubricant additives, and oil-based lubricants, to show the hydrodynamic and hydration contributions to liquid superlubricity. The review also discusses four methods to further expand superlubricity by solving the challenge of lubricants that have a high load-carrying capacity with a low shear resistance, including enhancing the hydration contribution by strengthening the hydration strength of lubricants, designing friction surfaces with higher negative surface charge densities, simultaneously combining hydration and hydrodynamic contribution, and using 2D materials (e.g., graphene and black phosphorus) to separate the contact of asperities. Furthermore, uniform mechanisms of liquid superlubricity have been summarized for different liquid lubricants at the boundary, mixed, and hydrodynamic lubrication regimes. To the best of our knowledge, almost all the immense progresses of the exciting topic, superlubricity, since the first theoretical prediction in the early 1990s, focus on uniform superlubricity mechanisms. This review aims to guide the research direction of liquid superlubricity in the future and to further expand liquid superlubricity, whether in a theoretical research or engineering applications, ultimately enabling a sustainable state of ultra-low friction and ultra-low wear as well as transformative improvements in the efficiency of mechanical systems and human bodies.

Keywords: liquid superlubricity; hydrodynamic lubrication; hydration lubrication; surface potential; surface forces

1 Introduction

Friction and wear are accompanied by many aspects of production and life, from the micro- to the macro-scale. Humans have been committed to reducing friction for thousands of years, saving energy and resources, protecting the environment, and improving service life [1–3]. According to incomplete statistics, nearly one-third of the world's disposable energy is wasted during the friction process [3, 4]. Approximately 80% of mechanical components and parts fail owing to friction and wear. Over 50% of mechanical equipment malignant accidents are related to lubrication failure during friction [5]. The annual economic losses of highly industrialized countries resulting from friction and wear are as high as 2% of the GDP value [4]. The global GDP was approximately 85 trillion dollars in 2020; and thus, the economic loss caused by friction is estimated to reach 2 trillion dollars. Therefore, research on lubrication to reduce friction and wear is necessary and has significant social, environmental, and economic benefits [6–8]. A significant theoretical

* Corresponding author: Chenhui ZHANG, E-mail: chzhang@tsinghua.edu.cn

breakthrough is the concept of superlubricity, originally proposed based on the Frenkel–Kontorova model by Hirano and Shinjo et al. [9–12] in the 1990s. It was used to describe a theoretical sliding state in which friction or resistance to sliding almost vanishes. By a widely accepted convention, superlubricity is used to describe the lubrication state, where the coefficient of friction (COF) is in the order of magnitude of 0.001 or lower. In the last three decades, significant progress has been made in solid and liquid superlubricity. Recently, superlubricity has become a research hotspot in fundamental science and engineering communities [13]. For solid lubrication materials, graphite, diamond-like carbon (DLC) films, multiwall carbon nanotubes, and two-dimensional (2D) materials such as molybdenum disulfide (MoS_2), graphene, and boron nitride have been found to exhibit superlubricity because of the weak interlayer interaction under specific conditions (such as temperature, humidity, and contact pressure) [14–22]. Liquid superlubricity can be divided into two types: water-based superlubricity and oil-based superlubricity. In this review, liquid superlubricity is discussed and summarized from fundamental phenomena and mechanisms to industrial applications.

To date, liquid superlubrication systems can be divided into five categories, as shown in Table 1. The first is water-and acid-based aqueous solutions. An ultra-low COF of 0.002 was obtained for water when two Si_3N_4 surfaces rubbed against each other at sliding speeds above 65 mm/s and contact pressures lower than 1 MPa using a pin-on-disk tribometer [23]. Subsequently, the superlubricity of water between SiC–SiC and Al_2O_3–Al_2O_3 was achieved with a minimum COF of 0.006–0.007 after a sliding distance longer than 1,000 m [24], and the running-in period was mainly influenced by the initial roughness of the ceramic surfaces [25]. In 2011, a novel superlubricity phenomenon of phosphoric acid (H_3PO_4) was observed between glass–Si_3N_4, sapphire–sapphire, and Si_3N_4–sapphire tribopairs after a running-in period of approximately 600 s using a universal micro-tribometer [26–28]. Next, an ultra-low COF of 0.004–0.006 for mixtures of acids and glycerol or polyhydroxy alcohols was obtained between the Si_3N_4–glass and Si_3N_4–sapphire interfaces [29–31]. For water and acid-based solutions, a lubrication film was formed to support the normal load and had a low shear resistance. That is, the hydrodynamic effect plays a key role in the superlubricity, and a hydrogen bond network helps to increase the viscosity of lubricants [27, 31].

To explore novel mechanisms to realize superlubricity, a few studies have been performed using a surface force apparatus or surface force balance (SFA or SFB), and the hydration effect was proposed to explain the extremely weak shear resistance of the hydrated materials between two mica surfaces [32]. Hydrated ions, phosphatidylcholine (PC) liposomes or bilayers, polymer brushes, and amphiphilic surfactants have all been confirmed to be superlubricating, and ultra-low

Table 1 Five different categories of liquid superlubrication systems.

Lubricant materials		$\overline{COF}$[1]	Pressure[2] (MPa)	Methods[3]
Water and acid-based solutions [23, 26, 31]		0.002−0.009	5	Tribometer, SFA
Hydrated materials	Hydrated ions [33, 53, 54]	10^{-4}−0.01	10–250	SFA, tribometer
	Phospholipids [37, 87, 88]	10^{-5}−0.002	40	SFA
	Polymer brushes [35, 46, 89]	10^{-4}−0.01	15	SFA, tribometer
	Surfactants [36, 90, 91]	10^{-4}−0.01	10	SFA, AFM
	Hydrogels [49, 50, 92–95]	0.001−0.01	1	Tribometer
Ionic liquids [45, 51, 52, 96, 97]		0.001−0.006	130	AFM, tribometer
2D materials as lubricant additives [64, 65]		0.0006−0.006	650	Tribometer
Oil-based lubrication [79, 83, 84, 86, 98–100]		0.001−0.008	100	Tribometer

[1] $\overline{COF}$ is the average coefficient of friction.

[2] Pressure represents the average contact pressure during superlubricity.

[3] SFA represents surface force apparatus, the same as surface force balance (SFB); AFM represents atomic force microscope.

COF of 10^{-5}–10^{-3} was obtained at maximum contact pressures of 1–30 MPa. This was attributed to a hydration layer [33–40]. The fluid hydration layer cannot only sustain a large normal load without being squeezed out but also retain the shear fluidity characteristic of the bulk liquid even under compression [32]. Based on recent studies, binary saturated and monounsaturated PC mixtures showed good boundary lubrication and rapid self-healing up to contact pressures of 5 MPa [41]. Sphingomyelin has also been found to be an excellent boundary lubricant in synovial joints, which is in parallel with PC [42]. Phytoglycogen nanoparticles exhibited striking boundary lubrication performance with a COF of 10^{-3} and excellent water retention because of the abundance of close-packed hydroxyl groups forming hydrogen bonds with water and then forming hydrated layers [43]. In particular, ionic liquids (ILs) exhibit efficient lubrication properties because of the irregular shapes of the ions and strong coulombic interactions between the ions and charged-confining surfaces at the microscale [44]. The superlubricity of ILs at the silica–graphite interface can be externally controlled by applying an electrical potential to the graphite surface using an atomic force microscope (AFM) because the IL is solely composed of cations and anions [45]. The combination of ILs and polymer brushes has been found to exhibit excellent lubrication characteristics. Concentrated polymer brushes immersed in two highly viscous ILs exhibited an ultra-low COF (< 0.001) between hydrophobized silica surfaces because of the small adhesive interaction between the two brush surfaces and hydrodynamic lubrication [46].

However, most experiments were conducted using SFA and AFM with atomically smooth surfaces (such as mica and graphite) under low contact pressures, and obtaining macroscale superlubricity of hydrated materials and ILs remains unresolved for a long time. Recently, breakthroughs have been made on macroscale superlubricity. The brush-like co-polyelectrolyte (PLL-*g*-PEG) adsorbed on oxide surfaces (FeO_x–SiO_x) and ceramic surfaces (Si_3N_4, SiC) showed low COF (< 0.01) with the speed increasing from 0.1 to 2.5 m/s using a pin-on-disk tribometer because a lubrication film with a thickness of above 10 nm was formed after a long running-in period; and thus the superlubricity was attributed to the hydrodynamic lubrication because the film thickness was larger than the composite surface roughness [47, 48]. Zwitterionic hydrogels had remarkable lubrication capabilities and showed a low COF of 0.002–0.006 under a normal load between 0.5 and 4 N. This was attributed to a hydrated layer on the hydrogel surfaces [49, 50]. Ultra-low COFs of 0.002–0.005 and 0.002–0.008 were achieved by hydrated ions and ILs between Si_3N_4–sapphire and Si_3N_4–Si_3N_4 interfaces, respectively, using a ball-on-disk tribotester under contact pressures of above 100 MPa [51–54]. The superlubricity of carbon quantum dots modified by ILs was achieved between silicon chips and steel or Al_2O_3 balls at an applied load of 20 mN using a rotating ball-on-disk tribotester [55].

However, a higher load-carrying capacity of liquid lubricants is necessary, especially in engineering applications. Based on previous studies, the final average contact pressures after achieving superlubricity are typically less than 300 MPa, and most of them are less than 10 MPa, even though the initial contact pressures are much higher (even up to 1 GPa), which results from mechanical wear and tribochemical reactions during the running-in period. According to the Hamrock–Dowson theory based on hydrodynamic lubrication, liquid superlubricity is influenced by the contact pressure between friction surfaces and the pressure–viscosity coefficient of the lubricant [56]. When the pressure–viscosity coefficient is less than 5 GPa^{-1}, liquid superlubricity can still be obtained at pressures above 500 MPa [57, 58]. Theoretically, it is possible for aqueous lubricants with low pressure–viscosity coefficients to achieve water-based superlubricity under high contact pressures. Recently, a novel comb-type polymer and aqueous PEG–salt mixtures achieved an ultra-low COF of approximately 0.005 under high contact pressures of above 350–500 MPa. This was attributed to the synergistic effect of hydration contribution and hydrodynamic lubrication [59, 60].

In addition, 2D materials have been used as high-performance liquid-phase lubricant additives [22, 61–63]. Superlubricity was achieved using a combination of graphene oxide (GO) nanosheets and an IL ([Li(EG)]PF_6) between Si_3N_4–sapphire interfaces under an extreme pressure of 600 MPa, which mainly

resulted from the high load-carrying capacity of the GO nanosheets and the low shear resistance between the GO nanosheet interlayers [64]. As a newcomer to 2D materials, black phosphorus (BP) nanosheets achieved an ultra-low COF of 0.0006–0.006 between Si_3N_4–SiO_2 interfaces under high contact pressures of up to 100 MPa after modification by NaOH (BP–OH), which resulted from the lamellar slip of BP–OH nanosheets and the low shear resistance of the water layer retained by BP–OH nanosheets [65–67]. In summary, to achieve liquid superlubricity, lubricants must exhibit two characteristics. The lubricant should have a low viscosity, which can shear easily while providing sufficient load support [68]. These findings laid the foundation for the analysis of the underlying superlubricity mechanisms in aqueous conditions.

In addition to the experimental studies, water-based superlubricity has also been studied at the atomic scale using molecular dynamics (MD) simulations. Leng et al. [69, 70] performed MD simulations to investigate the hydration structure of water and the shear dynamics of hydration water confined between mica surfaces (which are inert, atomically smooth, and easily prepared by cleavage in an ambient atmosphere [71]) at a pressure of 0.1 MPa and a temperature of 298 K. They found that the surface-bound hydration layers under nanoconfinement (with a distance of 0.9–2.4 nm) could remain fluid, as observed in SFA experiments, resulting in highly efficient superlubrication, which could be explained by the fast rotational and translational dynamics of water molecules in the hydration layers under confinement [69, 70]. Based on MD simulations, a repulsive hydration force and thus a high load-bearing capacity in aqueous KCl electrolyte solution was obtained within a distance of 2 nm between mica surfaces, which was attributed to the very hard hydration shells of K^+ cations under confinement [72, 73]. Through MD simulations in highly concentrated and confined aqueous NaCl solutions, the electric double-layer structure was sensitive to the distribution of surface charges, and a slight charge inversion appeared, which depended on the bulk concentration and surface charge density [74]. The charge inversion phenomenon at high concentrations was also observed in zeta-potential experiments, which was conducive to superlubricity [54]. However, most of the above simulation studies were performed around mica surfaces in aqueous solutions, which can only describe the interfacial and molecular interactions at high concentrations; however, it cannot reasonably simulate the interactions at low concentrations because of the confined simulation systems (which are usually in the nanoscale conditions). The mica surface loses K^+ ions at the interface when immersed in aqueous solutions and becomes negatively charged, which influences the initial concentration of the aqueous solutions [75]. The higher the concentration of the initial solution, the smaller the impact of the loss of K^+ ions on the concentration. For graphite, graphene, or titanium carbide surfaces, such a problem does not occur [76–78]. Therefore, a solution to the accuracy problem of concentration during MD simulations on mica surfaces at low concentrations may be worth considering in subsequent simulation studies.

Compared with numerous studies on water-based superlubricity, oil-based superlubricity can satisfy industrial applications and result in direct economic benefits. For oil-based lubrication, the pressures between friction pairs are mainly supported by the hydrodynamic lubrication film because of the higher viscosity and higher viscosity–pressure coefficient of oils. However, some breakthroughs to achieve oil-based superlubricity have also been made in recent years. Zhang et al. [79] and Li et al. [80, 81] found that the superlubricity of diketone lubricants can be obtained between steel surfaces because of the chemical adsorption layers formed on the rubbing surfaces through a tribochemical reaction occurring between the benzoylacetone and rubbing steel surfaces. Some studies also found the superlubricity of castor oils between Nitinol 60 alloy and steel surfaces, and the superlubricity of poly-α-olefin (PAO) oil between Si_3N_4–DLC films, as well as the superlubricity of glycerol between DLC or graphene-coated surfaces [82–84]. In addition, modified 2D materials (such as graphene) as novel lubricating additives in oils (such as PAO and polyalkylene glycol) can also achieve ultra-low friction, which is attributed to the tribochemical layer formed on the friction pairs and the hydrodynamic effect [85, 86]. More patience is needed to obtain oil-based superlubricity without

hydrodynamic contributions in the future.

The main purpose here is to summarize and review our research on liquid superlubricity in the past decade, and then to discuss the superlubricity mechanism based on our studies. Furthermore, considering the significant efforts made in liquid superlubricity from fundamental science and engineering applications in the last three decades, this review article aims to cover the developments and unlock the mechanisms of liquid superlubricity. Here, the initial discovery of liquid superlubricity is introduced, especially the acid-based superlubricity discovered in our laboratory, and then discuss methods and materials to further expand superlubricity from the well-known hydration superlubrication to novel 2D materials as new lubricant additives. In particular, the superlubricity phenomenon is summarized and uniform superlubricity mechanisms suitable for most water-based superlubricity systems are proposed. Finally, suggestions and an outlook for future research on liquid superlubricity are offered.

2 Initial discovery of liquid superlubricity

Since the discovery of superlubricity by water lubricating two ceramic surfaces in the 1990s, little progress has been made in the field of macroscale liquid superlubricity, and few superlubricating materials (including polysaccharide and polymer brushes) have been found [47–48, 101]. Thus, the development of liquid superlubricity seems slow in the following 20 years [102]. Energy is dissipated by disordered liquid molecules during shear because of entanglement and collision, resulting in high shear resistance. Meanwhile, disordered liquid molecules cannot form stable repulsion to sustain the normal load on friction surfaces [102–104]. Therefore, obtaining liquid superlubricity under high contact pressures (~100 MPa) and normal environmental conditions (room temperature, atmospheric pressure, and air atmosphere) remains a significant challenge unless the aforementioned problems can be solved. A significant breakthrough in the field of macroscale liquid superlubricity was made in the early 2010s (approximately 20 years after the first realization of ceramic–water–ceramic superlubrication) using phosphoric acid aqueous solution as well as mixtures of acids and glycerol as lubricants inspired by yogurt [26, 29, 103, 105]. An ultra-low COF of 0.003−0.006 was obtained between Si_3N_4–glass, Si_3N_4–SiO_2, Si_3N_4–sapphire, and ruby–sapphire interfaces under lubrication of an H_3PO_4 solution (pH = 0−1.5), mixed solutions (pH = 0−1.5) of inorganic or organic acids (H_3BO_3, H_2SO_4, HCl, $C_3H_6O_3$, $H_2C_2O_4$, $C_6H_8O_7$, and H_3NO_3S), and glycerin at a normal load of 0.5−10 N, corresponding to a final contact pressure of 50−230 MPa, as shown in Fig. 1(a) [26–29, 31, 106, 107]. In addition, water-based superlubricity was achieved with similar lubricants, such as mixtures of acids and polyhydroxy alcohols (including polyethylene glycol), after a running-in period of approximately 500 s [30, 108].

Since the discovery of acid-based superlubricity, the superlubricity mechanism has been explored. It has been shown through experiments before 2015 that two factors dominated the superlubricity (including friction, *in situ* Raman spectrum, and sum-frequency generation vibrational spectroscopy) as well as conjectures, such as H^+ ions in the lubricants and a network of hydrogen bond formed by water and acid molecules [106, 109–111]. However, tribological experiments and calculation showed that acid-based superlubricity was influenced by the contact pressure, sliding speed, and pressure–viscosity coefficient of lubricants, and the superlubricity of the H_3PO_4 solution failed when the sliding speed was less than 12−40 mm/s and the normal load was above 7−10 N [27, 28, 56, 112]. Therefore, it is reasonable to speculate that the hydrodynamic effect might play a significant role in the achievement of acid-based superlubricity. With the aid of an experimental setup for film thickness measurements based on the relative optical interference intensity, the *in situ* film thickness of lubricants during friction can be measured accurately with a high resolution in film thickness of 0.5 nm [27, 113]. As shown in the interference images at different times (Fig. 1(a)), a bright tail appeared at the outlet region of the contact area at 100 s, which resulted from the negative pressure at the outlet induced by the hydrodynamic effect. The COF and film thickness of the H_3PO_4 solution vs. sliding speed were measured simultaneously, as shown in Fig. 1(b). The COF decreased from approximately 0.3 to 0.003, and the film thickness (h) increased from 5–8 to 17 nm (and the

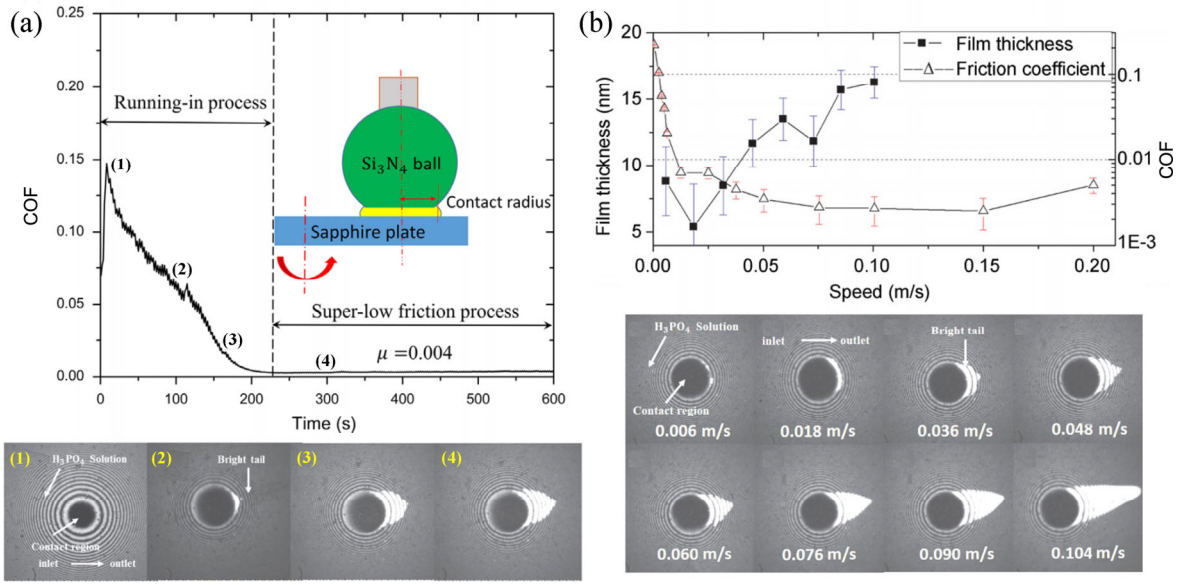

Fig. 1 Results of friction and film thickness of the H_3PO_4 solution (pH = 1.5) and a mixed aqueous solution of H_2SO_4 and glycerin (pH = 1.5) under a load of 1.5 N. (a) COF vs. time for a H_2SO_4 and glycerin (20%) mixture. The images below showed the contact area (sliding speed = 0.076 m/s) at (1) 10 s, (2) 100 s, (3) 170 s, and (4) 300 s, respectively. (b) Film thickness and COF as a function of sliding speed for the H_3PO_4 solution. The interference images below showed the contact area at different speeds. Reproduced with permission from Ref. [27], © the Author(s) 2014; Ref. [31], © Elseiver Ltd. 2016.

length of the bright tail was increased significantly) as the sliding speed increased from 6 to 100 mm/s. The equivalent surface roughness of the friction pairs (σ) was approximately 5 nm. According to the criteria (the thickness-roughness ratio $\lambda = h/\sigma$) to judge lubrication regimes [114] and the Stribeck curve (describing the relationship between COF and sliding speed), it can be inferred that acid-based solutions were in the mixed and elastohydrodynamic lubrication regimes during superlubricity. That is, hydrodynamic lubrication contributes significantly to acid-based superlubricity, which provides a complete understanding of acid-based superlubricity. It should be noted that the viscosity of the H_3PO_4 solution increased from 2–3 to 25 mPa·s as the concentration of H_3PO_4 molecules increased from 20% to 80% during the friction process from the running-in period to the superlubricity state. During superlubricity, the viscosity increased by 10 times. This was attributed to the evaporation of water and the formation of a hydrogen bond network, which led to an increase in the film thickness and an increase in the hydrodynamic lubrication [27]. In addition, the H^+ ions played two roles during the running-in period, such as reducing the surface roughness to form relatively smooth friction surfaces and assisting in the formation of an easy-to-shear silica layer through a tribochemical reaction [31, 115, 116], which also led to the increasing contribution of hydrodynamic lubrication. In summary, the acid-based superlubricity achieved by a series of acids and a combination of different acids and alcohols was mainly attributed to the contribution of the hydrodynamic effect, and the running-in period was essential for the achievement of superlubricity. Superlubricity with the lubrication of H_3PO_4 solution can also be obtained in a vacuum with a vacuum degree lower than 10^{-2} Pa, which was attributed to the phosphoric acid-water network and water molecules locked in the lubrication film even in a vacuum because of the interaction of the strong hydrogen bond [117].

The acid-based superlubricity can also be explained from the perspective of the Stribeck curve, as shown in Fig. 2. Three lubrication regimes can be identified according to the relationship between COF and the Sommerfeld number ($\eta v/p$, where η represents the viscosity, v represents the velocity, and p represents the contact pressure), such as boundary lubrication (BL), mixed lubrication (ML), and hydrodynamic or elastohydrodynamic lubrication (EHL). In the BL

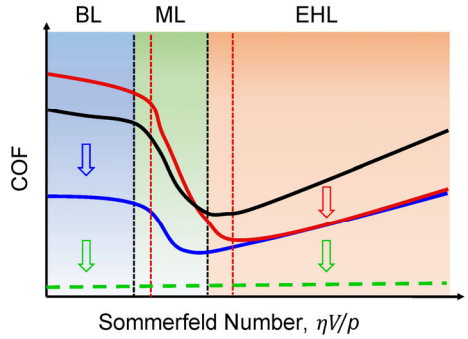

Fig. 2 Classical Stribeck curve with the lubrication regime identified (the black curve) and the methods to reduce friction (the red and blue curves). The red curve represents a reduction in the viscosity of lubricants, resulting in a decrease in COF in the EHL regime and an increase in COF in the BL regime, whereas the blue curve represents methods to reduce COF in the BL regime, such as the surface coating technique and surface grafting modification. Superlubrication (the green dot curve) is becoming the goal for researchers in the field of mechanics, physics, chemistry, material, and engineering.

regime, solid surfaces contact each other directly, and the load is mainly supported by the surface asperities; thus, high friction exists. However, the COF can be reduced by surface coating and surface grafting modification (the blue curve) [35, 47, 82, 118–121]. In the EHL regime, the fluid lubrication film completely separates two solid surfaces, and the load is mainly supported by the hydrodynamic pressure, where the friction is significantly influenced by the effective viscosity of the liquid confined in the contact area. Therefore, an effective method to reduce the COF in the EHL regime is to reduce the viscosity of lubricants; however, the decrease in viscosity will increase the COF at the BL and ML regimes (the red curve). In the ML regime, some surface asperities are in contact, and the load is supported by both surface asperities and lubrication film. The lowest COF is in the transition position between ML and EHL, where the thinnest fluid film lubrication is formed, which was also demonstrated through calculations based on elastohydrodynamic lubrication [56, 92]. It has been confirmed that acid-based superlubrication occurs in the ML and EHL regimes, which is in accordance with the prediction of the Stribeck curve. To the best of our knowledge, both high and low Sommerfeld number regimes should be considered to achieve super-low friction under a wide range of conditions (the green dot curve). Reducing the viscosity of lubricants is necessary to reduce the COF in the high Sommerfeld number regime (EHL regime); thus, aqueous lubricants will be better than oils because of the low viscosity of aqueous solutions [56, 99]. In addition, there are still some difficulties in obtaining superlubricity in the low Sommerfeld number regime (BL regime). In the BL regime, the friction force is mainly derived from the interactions between surface asperities. Therefore, the avoidance of direct contact between surface asperities is the key to obtaining superlubricity, which leads us to solve the question of how to share the normal pressures. This is challenging because the high load-carrying capacity and low shear resistance of lubricants are usually mutually exclusive; however, they are both necessary to achieve superlubricity. Significantly, the hydration effect and 2D materials with low interfacial shear strength have been proposed to exhibit super-low friction, which provides a novel method to extend liquid superlubricity.

3 Hydration contribution to liquid superlubricity

With the aid of SFA or SFB setups and atomically smooth mica surfaces, normal and friction forces are measured in aqueous solutions, and hydration repulsion and hydration lubrication effects have been observed to show extremely low friction [32, 34, 35, 122–125]. The water molecules and hydration layers (charges surrounded by water molecules) retain the shear fluidity characteristic of the bulk liquid between two mica surfaces confined to thin films of a few molecular layers, which is attributed to the rapid exchange of water molecules within the hydration shells and bulk solution during shear under strong compression [32, 124, 126]. The persistent fluidity of hydration layers nanoconfined between mica surfaces with a film thickness of 0.9–2.4 nm was also found through molecular dynamics simulations, resulting from the fast rotational and translational dynamics of water molecules under this extreme confinement [69, 70, 72]. Many hydrated materials (such as hydrated ions, charged and zwitterionic polymer brushes, surfactants, phosphatidylcholine liposomes or bilayers, and other biological macromolecules) have been found to exhibit striking lubrication properties because the hydration

layers can sustain large pressures without being squeezed out while retaining fluid response to shear with extremely low friction [125, 127, 128]. A sliding COF as low as 10^{-5}–10^{-3} was obtained between hydrophilic mica surfaces or even hydrophobic surfaces under mean contact pressures of up to 10–30 MPa [37, 129]. Inspired by hydration lubrication, it can be proposed that the hydration repulsive force can prevent the direct contact of the surface roughness peaks and bear the normal pressures. That is, a novel method of introducing the hydration effect into the macroscale lubrication was considered to obtain liquid superlubricity in a wider range of conditions (such as higher pressure, lower velocity, and rougher surfaces). Therefore, to obtain macroscale superlubricity under a boundary lubrication regime with a higher contact pressure above 100 MPa, tribological experiments were performed on hydrated ions using a ball-on-disk tribometer, as shown in Fig. 3. It can be seen that an ultra-low COF of 0.005 was obtained between Si_3N_4 and sapphire surfaces with the lubrication of three alkali metal salt solutions (Li^+, Na^+, and K^+) under high contact pressures above 250 MPa. This result agrees with the expectations of the Hofmeister series, where the lubrication is improved by enhancing the ionic hydration strength [53, 130]. An acid (such as H_3PO_4, HCl, and H_2SO_4) running-in period of 300 s was the basis of the superlubricity by hydrated ions (Fig. 3(c)), and it has also been found that the running-in period is necessary for most liquid superlubrication systems (such as ceramic–water–ceramic, ceramic–acid–ceramic, and steel–oil–steel systems) [31, 79, 131]. In addition, the hydrodynamic effect still plays a role in achieving the superlubricity of hydrated ions, because the COF increased to > 0.01 as the sliding speed decreased (Fig. 3(d)), meaning superlubricity under the boundary lubrication regime cannot be realized when the hydrodynamic effect weakens.

It has been demonstrated that a smooth worn region is formed during the running-in process, with a decrease in surface roughness and contact pressure,

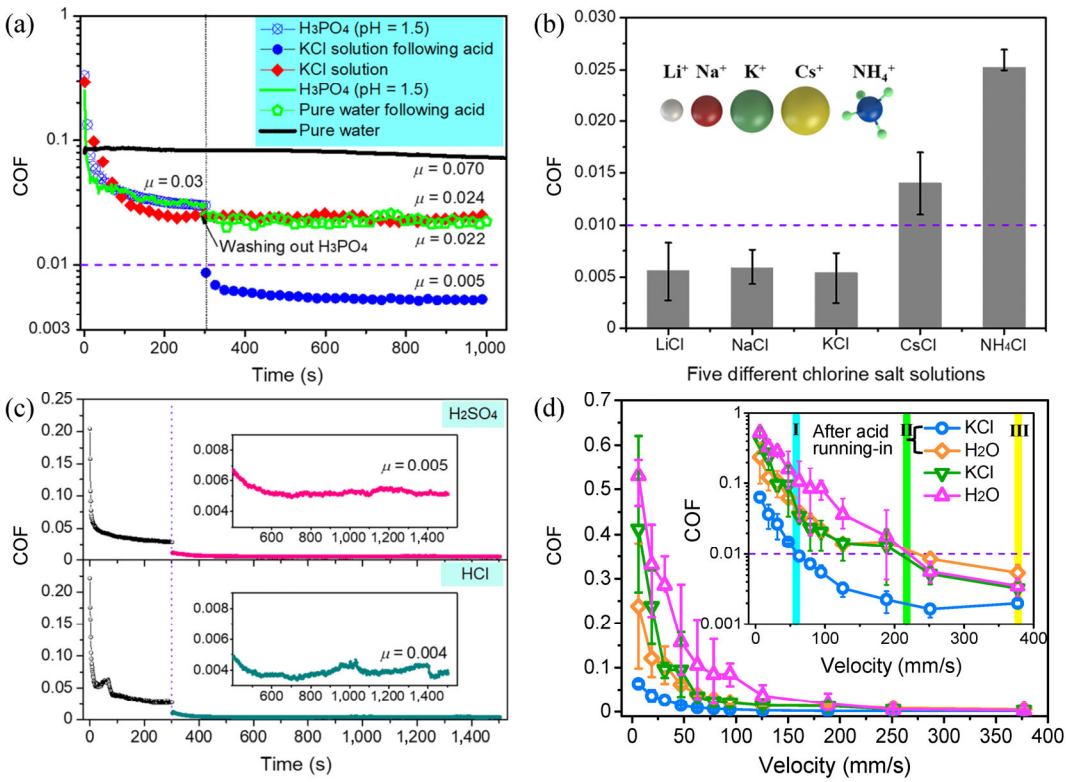

Fig. 3 Superlubricity of hydrated ions between Si_3N_4–sapphire interfaces under a normal load of 3 N: (a) COF of H_3PO_4 solution, KCl solution, and water with or without acid running-in. (b) Comparison of COF under lubrication of five different chloride salt solutions. (c) COF of KCl solution after running-in with H_2SO_4 and HCl solutions. (d) COF of KCl solution and water with or without acid running-in as a function of sliding speed. Reproduced with permission from Ref. [53], © American Chemical Society 2018.

thereby contributing to hydrodynamic lubrication [31, 132]. In addition, a tribo-induced silica layer was generated through a tribochemical reaction during the acid running-in period, and its amorphous structure and film thickness were resolved using transmission electron microscopy (TEM, Fig. 4(a)) and X-ray photoelectron spectroscopy (XPS) depth profile technique, which was consistent with previous findings [31, 132]. The silica layer was softer and had a lower elastic modulus of approximately 75 GPa (1/4 of Si_3N_4's elastic modulus), which resulted in less shear resistance during boundary lubrication, and the COF of Si_3N_4 with a silica layer was reduced by 55% to 130% compared to that without a silica layer [115]. Furthermore, the formation of a silica layer increased the density of hydroxyl groups (–OH) on the Si_3N_4 surface, thereby increasing the surface negative potential (the surface negative charge density increased by over 50%) and hydrophilicity (the contact angle decreased from 77°–85° to 61°–67°), which was confirmed by ζ-potential (Fig. 4(b)) and contact angle measurements. Therefore, more hydrated cations can be adsorbed on negatively-charged ceramic surfaces, which enhances hydration lubrication to achieve superlubricity. Figure 4(c) shows that superlubricity can only be obtained when the pH of the KCl solution is above 5, and the COF increases to above 0.01 with a decrease in pH below 5. Because the isoelectric points (IEPs) of Si_3N_4 and sapphire were both located at pH = 4.3 ± 0.3, it can be concluded that the superlubricity of hydrated ions can be achieved only when the friction surfaces are both negatively charged, which further proves that the hydration effect plays a key role in the achievement of superlubricity [53, 115]. In summary, not only the surface roughness and contact pressure decreased (contributing to the hydrodynamic lubrication), a tribo-induced silica layer was also generated during the running-in period. Two main roles of the silica layer have been reported to achieve superlubricity. First, the silica layer exhibits excellent friction-reducing properties under boundary lubrication at both the macroscale and microscale levels. Second, the silica layer has a larger negative surface charge density and better hydrophilicity, resulting in increased adsorption of hydrated cations on ceramic surfaces (contributing to hydration lubrication).

4 Further expansion of superlubricity

In essence, a high load-carrying capacity and a low shear resistance are necessary to achieve liquid superlubricity. The challenge is that it is usually incompatible and mutually exclusive for lubricants to exhibit both high load-carrying capacity and low shear resistance [68]. Therefore, the determination of methods to overcome this challenge is the main focus to obtain superlubricity in previous studies; thus, water and aqueous solutions with low viscosity are usually used as lubricants. In addition, previous studies on superlubricity show that smooth surfaces (with a surface roughness lower than 10 nm) were typically formed during superlubricity because of the early running-in period [27, 53, 132]. To the best of our knowledge, further expansion of liquid superlubricity, whether in theory or engineering applications, is worth exploring [68, 111]. Two key questions are proposed to extend the liquid superlubricity (including phenomena and mechanisms).

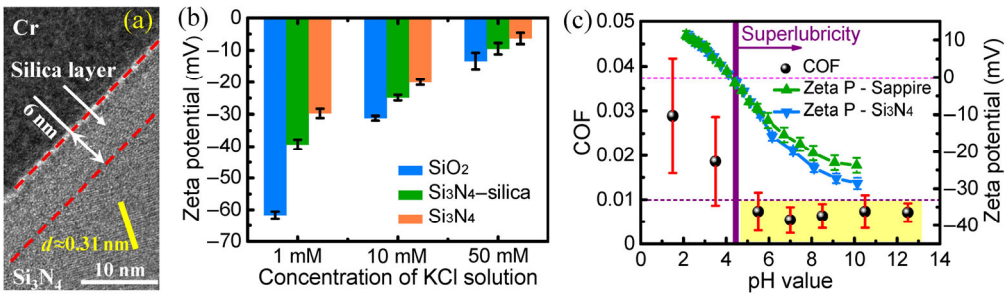

Fig. 4 A tribo-induced silica layer contributes to hydration lubrication: (a) TEM image showing the cross-section of the worn region on the Si_3N_4 ball after running-in with H_3PO_4 solution. (b) Comparison of ζ-potential for three different plates in neutral KCl solutions (pH = 5.3 ± 0.2). (c) COF of KCl solution as well as the ζ-potential of sapphire and Si_3N_4 as a function of pH value for a KCl solution of 50 mM. Reproduced with permission from Ref. [115], © American Chemical Society 2019.

1) How to obtain liquid superlubricity under a wider range of conditions (such as higher contact pressure, lower sliding velocity, and shorter running-in time) is important, which will have a significant impact on engineering applications based on liquid lubrication.

2) The hydrodynamic effect plays a key role in superlubricity in the hydrodynamic lubrication regime. In the boundary and mixed lubrication regimes, exploring novel methods to separate the friction surfaces or surface asperities apart from the hydration effect is valuable, which might contribute to obtaining novel superlubricity systems.

Recently, studies have been conducted to answer the first question. Figure 3(d) indicates that an ultra-low COF could only be obtained when the velocity was higher than 220 mm/s for water and KCl solution between Si_3N_4 and sapphire surfaces. After running-in in an acid solution, the lowest velocity to achieve superlubricity decreased to approximately 60 mm/s for the KCl solution. With the finding that a stronger hydration strength leads to better lubrication and less friction, that is the lubrication property of the salt solution is in agreement with the expectation analogous to the Hofmeister series [53, 124, 133], multivalent ions can be expected with a higher hydration strength to exhibit better lubrication characteristics. Recently, friction measurements of multivalent salt solutions were conducted between Si_3N_4 and sapphire surfaces [54], as shown in Fig. 5. All five different trivalent cations (Al^{3+}, Ce^{3+}, Cr^{3+}, La^{3+}, and Sc^{3+}) at high concentrations (1 M) exhibited superlubricity with a COF of 0.002–0.004 under contact pressures above 250 MPa. Three divalent alkaline-earth metal cations (Mg^{2+}, Ca^{2+}, and Sr^{2+}) at a high concentration (1 M) also achieved an ultra-low COF of 0.005–0.006. However, at a lower concentration (50 mM), both trivalent and divalent ions showed higher COFs under the same load and velocity, because adhesion rather than hydration repulsion existed between two negatively-charged surfaces in salt solutions at concentrations lower

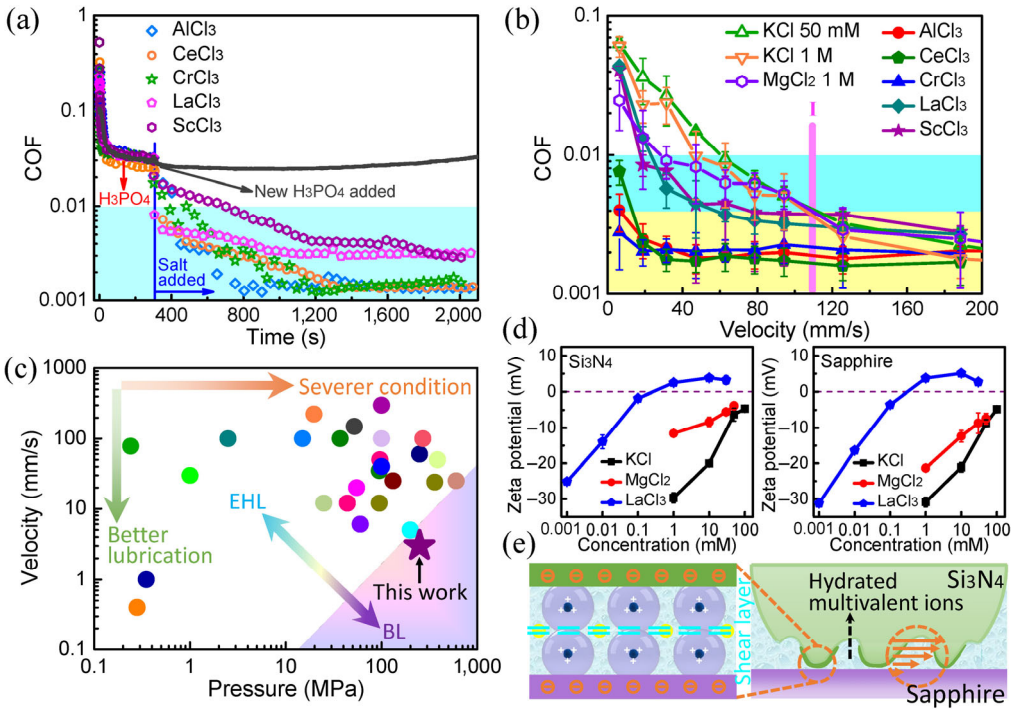

Fig. 5 Superlubricity of multivalent ions. (a) COF of 1 M trivalent chloride solutions after running-in with H_3PO_4 solution (pH = 1.5). (b) COF of monovalent (KCl, 50 mM and 1 M), divalent ($MgCl_2$, 1 M), and trivalent ($AlCl_3$, $CeCl_3$, $CrCl_3$, $LaCl_3$, and $ScCl_3$, 1 M) chloride solutions as a function of velocity. (c) Relationship between the lowest velocity to achieve superlubricity and the average contact pressure in this study and previous studies. EHL and BL denote elastohydrodynamic lubrication and boundary lubrication, respectively. (d) ζ-potentials of Si_3N_4 and sapphire as a function of concentration in KCl, $MgCl_2$, and $LaCl_3$ solutions. (e) Schematic of the lubrication model to reveal the mechanism of the superlubricity enabled by hydrated multivalent ions. Reproduced with permission from Ref. [54], © American Chemical Society 2019.

than the critical hydration concentration. That is, the hydration layers will be easier to squeeze out under confinement at lower concentrations [134, 135]. Because the higher the hydration strength, the better the lubrication performance is, it can be speculated that multivalent ions with higher hydration strength can realize ultra-low friction at lower velocities, which was confirmed by the velocity-dependent COF (Fig. 5(b)). The lowest velocity to achieve superlubricity for 1 M KCl, $MgCl_2$, and MCl_3 (M represents Al, Ce, and Cr) was 45, 30, and 3 mm/s, respectively. Trivalent ions, including Al^{3+}, Ce^{3+}, and Cr^{3+}, showed the best lubrication performance over a wide range of velocities (3–500 mm/s), and monovalent K^+ ions showed the worst lubrication performance in the low-velocity (< 110 mm/s) regime. According to Fig. 5(c), compared with previous studies, hydrated multivalent ions can achieve superlubricity at a relatively low velocity (3 mm/s) under a high contact pressure (250 MPa), resulting from the synergistic effect of hydration lubrication and hydrodynamic lubrication (Fig. 5(e)). On the one hand, hydrated ions are adsorbed strongly on negatively-charged ceramic surfaces; thus, the hydration lubrication contributes to the superlubricity, as demonstrated by SFA [32, 33] and ζ-potential measurements (Fig. 3(d)). On the other hand, the hydrodynamic effect also plays a role in the achievement of superlubricity owing to the existence of the lubrication film between solid surfaces, which is verified by the velocity-dependent friction (Fig. 5(b)) and film thickness calculation (the average film thickness was approximately 1–6 nm at a velocity of 50–500 mm/s under a normal load of 3 N) [54]. In summary, the macroscale liquid superlubricity was extended to a wider range of velocities from below 3 to above 500 mm/s under high contact pressures by enhancing the hydration strength of multivalent ions. Subsequently, the achievement of superlubricity with shorter running-in time at high contact pressure was investigated based on our previous findings (including macroscale hydration superlubricity [53, 54, 115, 136] and acid-based superlubricity [26–31, 103, 106–109]).

A running-in period ($\geqslant$ 300 s) is a necessary prerequisite to achieving macroscale hydration superlubricity and acid-based superlubricity. Generally, a long running-in period leads to serious wear on friction surfaces. To reduce wear and improve the service life of the equipment, the running-in time should be reduced. Recently, this limitation was overcome through the active design of aqueous mixtures of hydrated ions and polyethylene glycol (PEG) solutions; thus, the hydration and hydrodynamic contributions were combined [60]. As shown in Fig. 6(a), the COF of the PEG300–KCl mixture decreased from 0.15 to 0.004 with a running-in time of less than 1 min. The Si_3N_4 ball had the lowest wear rate after lubrication with the PEG300–KCl mixture, compared with the other three control lubricants, because of the lowest running-in time. The superlubricity of PEG–salt mixtures can be achieved at different mass fractions and concentrations of PEG and salts under a wide range of normal loads (1–9 N) and velocities (0.05–0.5 m/s). An ultra-low COF of 0.003–0.004, along with a short running-in time of less than 1 min, was obtained with the lubrication of aqueous mixtures of PEG300 and monovalent and multivalent chloride salt solutions (Fig. 6(b)). The mixed solutions of KCl and PEG with different molar masses of 200–1,000 g/mol also exhibited ultra-low friction, and the running-in time increased slightly from 40 to 150 s with an increase in the PEG molar mass from 200 to 1,000 g/mol owing to the increased viscosity of the mixtures (Fig. 6(c)). Therefore, rapid superlubricity was achieved using the PEG–salt mixture under high contact pressures of 500–600 MPa, and the Si_3N_4 ball had significantly low wear, and the sapphire disk had almost no wear because of the short running-in period, which was much shorter than that in previous findings, as shown in Fig. 6(d) [82, 86, 117, 137]. In the PEG–salt solution, hydrated cations can adsorb strongly on the negatively-charged ceramic surfaces, thereby favoring hydration lubrication, and PEG molecules retain random coils filling the bulk of the interfacial film, significantly increasing the viscosity of the mixed lubricants; thus contributing to hydrodynamic lubrication [60, 138]. In summary, superlubricity can be obtained at a low velocity of 3 mm/s with a rapid running-in under high contact pressures (> 250 MPa), by simultaneously enhancing the hydration strength and combining the contribution of hydration and hydrodynamic lubrication [60].

Because of these facts, hydrodynamic lubrication can be improved by increasing the viscosity of lubricants to a certain extent, and hydration lubrication can be

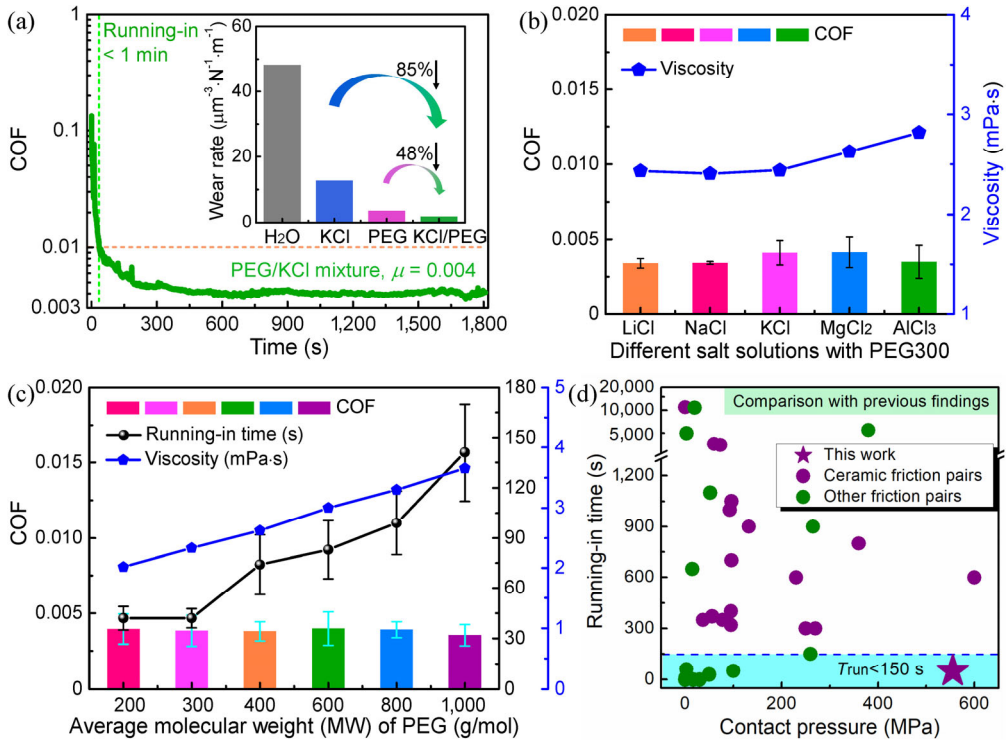

Fig. 6 Superlubricity obtained with mixtures of hydrated ions and PEG solutions between Si_3N_4 and sapphire surfaces: (a) COF of the PEG–KCl mixture as a function of time and the wear rate of Si_3N_4 balls after 30 min friction tests with the lubrication of four different lubricants; (b) COF and viscosities for mixed solutions of PEG300 and five different salts (LiCl, NaCl, KCl, $MgCl_2$, and $AlCl_3$); (c) COF and viscosities for mixed solutions of KCl and PEG with different average molar mass; and (d) relationship between the running-in time and the average contact pressure in this study and previous studies. Reproduced with permission from Ref. [60], © Elsevier Inc. 2020.

enhanced by increasing the hydration strength of cations. Furthermore, hydration lubrication can be achieved by adsorbing hydrated ions on charged solid surfaces without being squeezed out of the contact area under confinement. Therefore, in addition to enhancing the ionic hydration strength (which is the intrinsic property of ions), hydration lubrication can also be improved by increasing the surface charge density of friction surfaces because more counterions will be adsorbed on the charged surfaces. To further examine whether lubrication can be improved by enhancing the surface charge density, which can be assessed by the IEP, a new material was synthesized by grafting carboxylate anions ($RCOO^-$) into an epoxy resin matrix for tribological experiments [139]. Compared with the pristine epoxy resin (IEP = 6), modified epoxy resins with lower IEP of 3.8 and 3 exhibited better lubrication properties at low velocities of 1.2–94.2 mm/s (Figs. 7(a) and 7(b)). The modified epoxy resin with a lower IEP of 3 showed better lubrication properties than that with a higher IEP of 3.8. Figure 7(c) shows the COF of the modified epoxy resin (IEP = 3.8) rubbing past the sapphire surface under lubrication with water and NaCl solution and in dry friction. The COF increased with an increase in velocity in dry friction owing to the much more severe collision and wear of the asperities. In contrast, the COF increased with a decrease in velocity under the lubrication of water, indicating that the hydrodynamic lubrication weakened at lower velocities. As expected, the modified epoxy resin exhibited the lowest COF under lubrication with NaCl solution over the entire range of velocities, showing that ultra-low friction mainly resulted from hydration lubrication rather than hydrodynamic lubrication, especially at low velocities. In addition, the pH of the lubricants had a significant effect on the zeta potential of the epoxy resin, and all the epoxy resins had a higher negative surface potential at higher pH because more carboxyl and hydroxyl groups of the modified epoxy resin

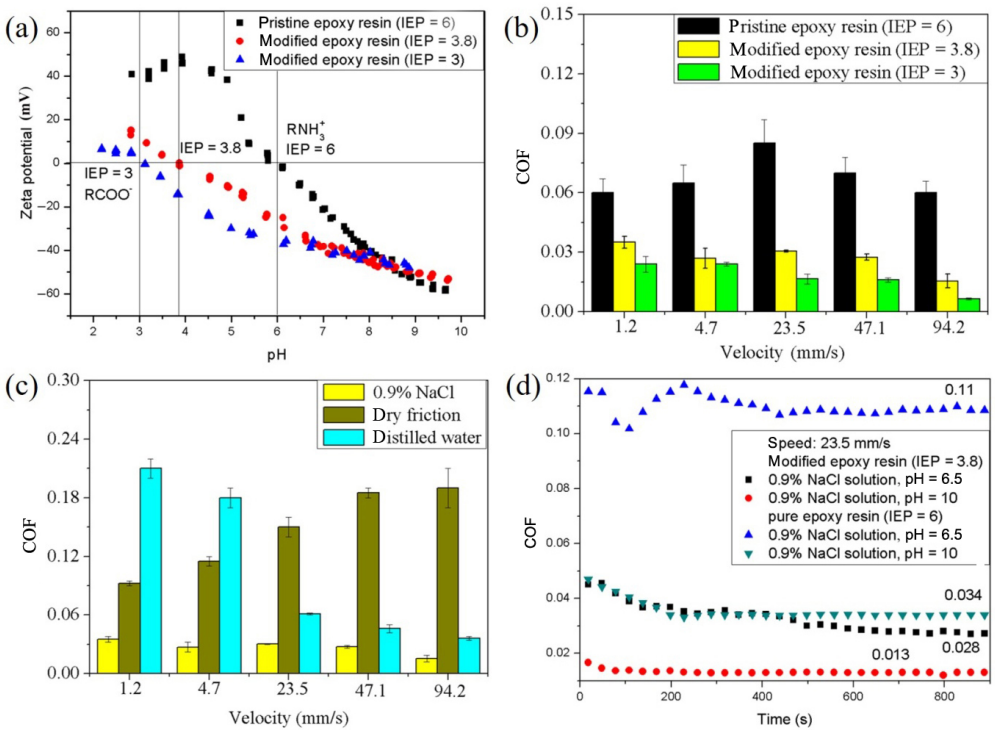

Fig. 7 Ultra-low friction obtained by modified epoxy resins: (a) ζ-potential of pristine and modified epoxy resins; (b) COF of pristine and modified epoxy resins vs. the velocity under lubrication of 0.9% NaCl solution; (c) COF of modified epoxy resins (IEP = 3.8) under dry friction and lubrication of water and 0.9% NaCl solution; and (d) pH effect of NaCl solution on the COF of pristine and modified epoxy resins. Reproduced with permission from Ref. [139], © WILEY-VCH Verlag GmbH & Co. KGaA, Weinhei 2020.

were ionized. Hence, it can be speculated that a lower COF of epoxy resin can be obtained under lubrication with an alkaline aqueous solution, which was proven by friction experiments, as shown in Fig. 7(d). Both the pristine and modified epoxy resins exhibited lower COF under lubrication with NaCl solution at a pH of 10 (alkaline) compared with that of 6.5 (neutral), because more hydrated cations were adsorbed on solid surfaces with higher negative surface charge density, which was also consistent with previous findings (Fig. 4(c)). In summary, a new method was developed to significantly reduce friction by enhancing hydration lubrication by improving the negative surface charge, that is, a negatively-charged material was designed by grafting negatively-charged carboxylate radicals into the epoxy resin matrix [139]. This result is consistent with the previous finding that the Si_3N_4 surface coated by a tribo-induced silica layer with a large negative charge potential had a prominent function of friction reduction [115].

Regarding the design of friction surfaces with high negative surface charge density to expand superlubricity, the effect of cation bridging on water-based lubrication as well as specific ion effects on polymers was discussed. In general, the grafted polyelectrolyte chains can be cross-linked by multivalent counterions, resulting in the collapse of polyelectrolyte brushes upon the addition of multivalent counterions, triggered by a significant reduction in osmotic pressure in the brushes [140]. Through SFA experiments, Yu et al. [141, 142] found that multivalent cations (Y^{3+}, Ca^{2+}, and Ba^{2+}), even at minute concentrations, could diminish the lubricity of polyelectrolyte brushes in aqueous solutions, resulting from the interchain interactions and structural properties of brush layers influenced by multivalent counterions, that is, electrostatic bridging and brush collapse caused by multivalent ions. Unlike polyelectrolyte brushes, zwitterionic bottlebrush polymers exhibited an ultra-low COF of 0.001 in the presence of multivalent cations (Y^{3+} and Ca^{2+}). Adibnia et al. [143] found that this superlubricating ability persisted until surface wear occurred at high normal pressures (below 1 MPa), and the surface wear was triggered by multivalent cations bridging the

polymer chains and dehydrating the zwitterionic moieties. However, compared with polymer brushes, the negatively-charged friction surfaces designed by our group (a charged bulk material, modified epoxy resin with a compressive strength of approximately 38 MPa and tensile strength of approximately 8 MPa) have much higher stiffness and strength; that is, no collapse behavior can be predicted for these designed negatively-charged surfaces in the presence of monovalent and multivalent counterions [139]. That is, an effective method was provided to solve the problem of cation bridging, which may lead to the failure of superlubricity in aqueous solutions with polymer brushes and counterions, that is, designing solid surfaces with high negative surface charge densities.

The first question proposed in Section 4 has been solved, and the second question will be answered. In the boundary and mixed lubrication regimes, both hydrodynamic lubrication and asperity contact are present, and friction increases owing to the surface roughness and asperity contact. Therefore, separation of the solid surfaces by lubricant molecules is a potential method to reduce friction. In addition to hydration layers composed of hydrated materials (including hydrated ions, polymer brushes, amphiphilic surfactants, and phosphatidylcholine liposomes or bilayers) [53, 54, 91, 144–147], 2D materials have reignited excitement in the tribology community owing to their excellent tribological properties, especially their capacity to separate two solid surfaces along with low shear resistance [22, 61, 63, 148]. Some 2D materials, such as graphene and black phosphorus improve lubrication and wear protection performance as additives in water-based lubricants, as shown in Fig. 8. The friction and wear rate were both reduced by depositing graphene family nanoflakes onto SiO_2 substrates [82]. An ultra-low COF of 0.004–0.015 was obtained between the Si_3N_4 ball and SiO_2 substrates with graphene coatings, including pristine grapheme (PG), fluorinated grapheme (FG), and GO nanoflakes under lubrication of aqueous glycerol solutions at a velocity of 0.1–0.2 m/s (Fig. 8(a)). A tribofilm composed of graphene nanoflakes on friction surfaces played a key role in achieving ultra-low friction (Fig. 8(b)). In addition, superlubricity can be achieved under lubrication of mixtures of GO nanosheets and polyhydroxy alcohol solutions, as well as mixtures of GO nanosheets and ILs, even under a high contact pressure of 600 MPa (Fig. 8(c)) [64, 149]. The adsorption layer of GO nanosheets on friction surfaces was conducive to the transformation of the shear interface from the Si_3N_4–sapphire interface into the GO–GO interface, and the excellent anti-wear property, extremely low shear stress, and high load-carrying capacity contributed to the achievement of superlubricity under extreme pressures [64, 76, 150–152].

BP, as a rising star in 2D materials, has been used as a water-based and oil-based lubricant additive because of its outstanding resistance to extreme pressures and high load-bearing capacity [153, 154]. BP modified by NaOH (BP–OH) is a high-performance water-based lubricant additive and showed an ultra-low COF of approximately 0.001 (Fig. 8(d)), resulting from the low shear resistance of the water molecules retained by the BP–OH nanosheets [65–67]. Subsequently, black phosphorus quantum dots (BPQDs) were prepared using the liquid-based high-energy ball milling method, and the BPQDs were stably dispersed in ethylene glycol [155]. An ultra-low COF of 0.002 was obtained with the lubrication of an aqueous BPQD–EG suspension between the Si_3N_4–sapphire interface (Fig. 8(e)). The rolling effect of the BPQDs and the low shear resistance between the BPQD interlamination, as well as the oxidative products (P_xO_y) of the BPQDs contributed to the achievement of superlubricity along with the improvement of wear protection performance (Fig. 8(e)). Recently, superlubricity under ultra-high contact pressure (> 1 GPa) was realized by lubrication with partially oxidized BP nanosheets at the Si_3N_4–sapphire interface, which was attributed to the abundant P=O and P–OH bonds formed on the oxidized BP nanosheets [156]. In addition, BP as an oil-based nanoadditive in oleic acid showed macroscale superlubricity at the steel–steel contact [157]. Therefore, 2D materials are an effective lubricant additive (which can also be used as anti-friction and anti-wear coatings on solid surfaces under liquid lubrication), which can generate a tribofilm on friction surfaces or form an adsorption layer; thus transferring the shear plane from the solid–solid interface to a 2D material–2D material interface with a low shear resistance. Meanwhile, 2D materials show excellent load-carrying capacities and can be present between

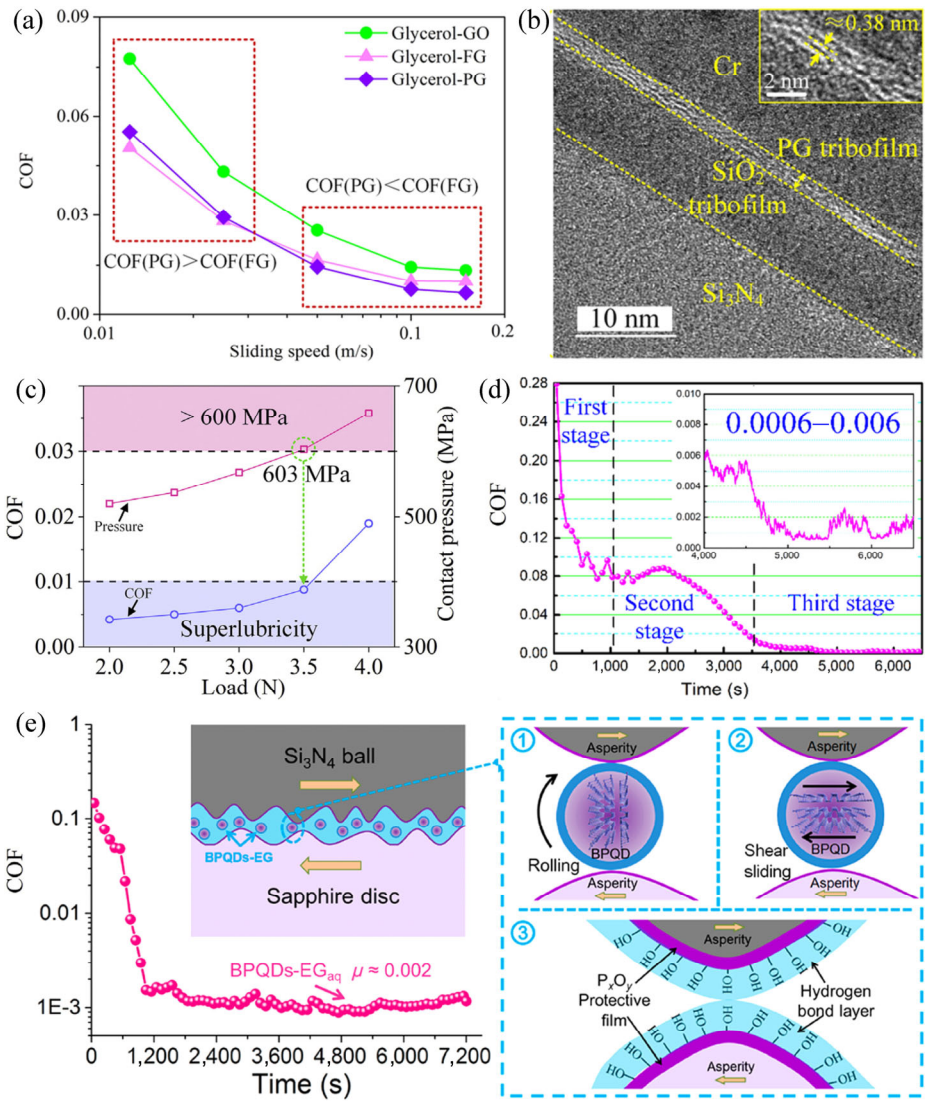

Fig. 8 Superlubricity obtained by 2D materials as additives and coatings in aqueous solutions. (a) COF vs. velocity under lubrication of glycerol between Si_3N_4 and SiO_2 surfaces with different graphene coatings. (b) High-resolution transmission electron microscopy image of the tribofilm on the Si_3N_4 ball. Reproduced with permission from Ref. [82], © American Chemical Society 2020. (c) COF and corresponding contact pressures between Si_3N_4 and sapphire surfaces under the lubrication of mixtures of an *in situ* formed IL ([Li(EG)]PF_6) and GO aqueous solutions. Reproduced with permission from Ref. [64], © Elsevier Ltd. 2019. (d) COF vs. time under the lubrication of black phosphorus modified by NaOH (BP–OH) solutions between Si_3N_4 and SiO_2 surfaces. Reproduced with permission from Ref. [65], © American Chemical Society 2018. (e) COF vs. time under lubrication of black phosphorus quantum dots mixed with ethylene glycol solution between Si_3N_4 and sapphire surfaces. Reproduced with permission from Ref. [155], © American Chemical Society 2020.

the contact area even under extremely high pressures. For solid lubrication, more 2D materials and heterostructures have offered potential opportunities to achieve superlubricity under specific conditions, including carbon nanotubes, molybdenum disulfide (MoS_2), graphene, graphite, and DLC, because of their weak interlayer interaction [17, 18, 21, 152, 158–162]. However, only a few 2D materials exhibit liquid superlubricity owing to limitations such as stable dispersion and interactions with oxygen and water [163]. The extension of liquid superlubricity with 2D materials as additives and coatings is an important direction for future research on tribology. In addition, it should be noted that for graphene or BP, superlubricity will fail at low speeds (Fig. 8(a)), which shows that the hydrodynamic effect should not be neglected

but plays an important role in the realization of liquid superlubricity with 2D materials.

5 Mechanisms of liquid superlubricity

Several materials have been found to obtain liquid superlubricity over the past 30 years, and much attention has been paid to exploring and analyzing the mechanisms behind lubrication systems. Although superlubricity mechanisms appear to be complicated, they should be further discussed. The key significance of this review is to unlock the mechanism behind liquid superlubricity, and pave the way for studies on new green lubricants and engineering applications of superlubricity. Generally, there are three lubrication regimes as defined from the Stribeck curve: boundary lubrication, mixed lubrication, and hydrodynamic lubrication (Figs. 2, 9(a), and 9(b)) [114, 164]. In the hydrodynamic lubrication regime, the load is supported mainly by the hydrodynamic pressure owing to negligible asperity contact, and the hydrodynamic pressure is generated by forming a converging wedge of fluid and forming a lifting pressure (Fig. 9(b)). According to the Sommerfeld number, $\eta v/p$, a reduction in the viscosity of the lubricant is the most effective method to reduce the friction in the hydrodynamic lubrication regime (Fig. 2); thus, low-viscosity fluids, especially water-based lubricants, have shown ultra-low COF below 0.01 at a specific range of pressure and velocity. However, in the boundary and mixed lubrication regimes, the asperity contact is present, and the load is supported by both surface asperities and the lubricants; thus, high friction is expected (Figs. 2 and 3(d)), which explains why the hydrodynamic effect cannot be neglected. To reduce the friction caused by surface asperities sliding past each other, it is necessary to determine methods of separating the asperities by low-viscosity fluids. That is, the major challenge is to explore lubricants with low viscosities or shear resistances along with high load-carrying capacities that cannot be squeezed out under pressure. Therefore, most studies on liquid superlubricity have focused on the determination of methods to overcome this limitation, typically using water and water-based solutions [68].

Here, the effect of separating surface asperities in contact at the boundary and mixed lubrication regimes is called the separating effect. The hydration effect is an effective method of separating the two surfaces and assists to obtain superlubricity. Using

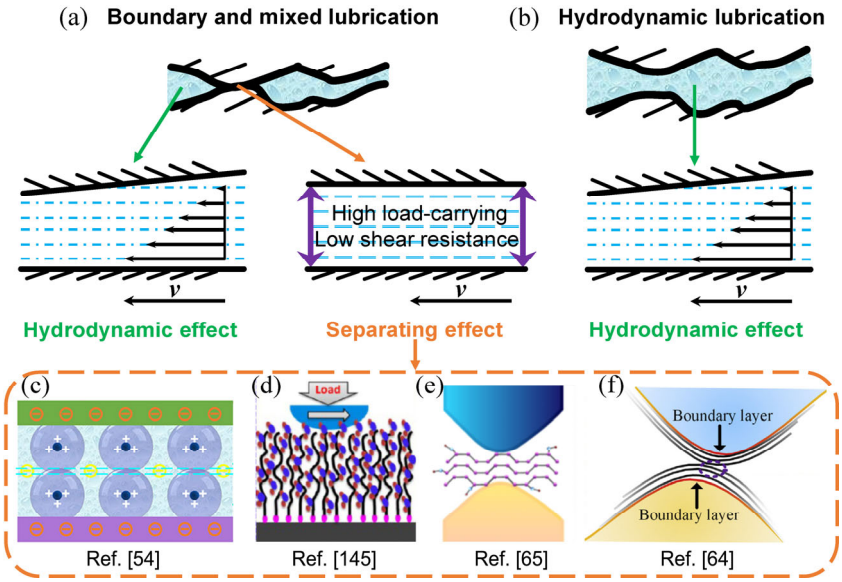

Fig. 9 Superlubricity mechanisms at (a) boundary and mixed lubrication, as well as (b) hydrodynamic lubrication regimes. Effects of separating two surfaces or asperities in contact at boundary and mixed lubrication regimes (called separating effect here), including hydration effects such as (c) hydrated ions [54] and (d) polyelectrolyte brushes [144], and 2D materials as additives such as (e) BP nanosheets modified by NaOH [65] and (f) GO nanosheets [64]. Reproduced with permission from Ref. [54], © American Chemical Society 2019; Ref. [145], © American Chemical Society 2013; Ref. [65], © American Chemical Society 2018; and Ref. [64], © Elsevier Ltd. 2019.

SFA or SFB, a hydration force is observed between atomically smooth mica surfaces in aqueous hydration solutions, which leads to hydration lubrication with ultra-low friction because of the hydration layers [32, 124, 125]. Hydration layers can support high pressures and overcome van der Waals attraction without being squeezed out, and show a fluid response to shear because of the ready exchange of water molecules within the hydration layers, as shown in Figs. 9(c) and 9(d) [54, 145]. In addition to hydrated materials with excellent hydration lubrication properties, 2D materials as lubricant additives and coatings exhibit outstanding anti-friction and anti-wear characteristics because of their high specific surface area, in-plane strength, weak layer–layer interaction, and surface chemical stability, as shown in Figs. 9(e) and 9(f) [63–65]. Based on the above discussion, the mechanism of liquid superlubricity at different lubrication regimes was proposed, as shown in Fig. 9, which has been proven to be able to explain most liquid superlubricity phenomena.

According to Fig. 9, the mechanism of liquid superlubricity can be clearly described based on the lubrication regime and Stribeck curve, which depends on several parameters, including the contact pressure, sliding velocity, surface roughness, viscosity of lubricants, and pressure–viscosity coefficient of lubricants. The hydrodynamic effect plays a key role in the EHL regime, where the thickness of the fluid film increases with increasing velocity or viscosity until the contact surfaces can be completely separated. Fundamentally, the aim of studying superlubricity is to solve the question of how to obtain superlubricity in the BL and ML regimes. Previous studies have demonstrated that interfaces lubricated by low-viscosity fluids can exhibit a lower-than-expected COF under certain conditions involving a high load-carrying capacity, a thin liquid film with low viscous friction, and smooth surfaces. However, the major challenge is that the first two are usually mutually exclusive (that is, how to support a large normal load and simultaneously have a low shear resistance for lubricants). Thus, most previous studies on liquid superlubricity have focused on finding methods to overcome this challenge, especially using water-based lubricants. For hydrated materials, hydration layers can simultaneously support large contact pressures without being squeezed out and exhibit a fluid response to shear; thus, superlubricity based on hydration contribution can be achieved at micro- and macro-scale conditions. For ILs, the irregular shapes of the ions inhibit solidification and locking, leading to low shear stress, whereas strong Coulombic interactions between the ions and the confined charged surfaces provide load support; thus, superlubricity can be obtained with ILs between atomically smooth mica and graphite surfaces [68]. For 2D materials as lubricating additives, sufficient load support and low shear resistance both assist in achieving water-based superlubricity under macroscale conditions. In summary, the next step to superlubricity is to continue finding an interface that is strong in the normal direction and weak in the shear direction. Baykara et al. [68] also proposed this concept three years ago.

To better analyze previous superlubricity phenomena using the mechanism proposed above (Fig. 9), the timeline of major milestones in research on liquid superlubricity was summarized, as shown in Fig. 10. According to the contact area and contact pressure, liquid superlubricity can be divided into microscale (typically AFM and SFA experiments) and macroscale (typically ball-on-disk and pin-on-disk tribometer experiments) superlubricity. Under microscale conditions, several fluids exhibit superlubricity, including hydrated materials [32, 34–37], alkane fluids [165–167], and ILs [45, 97]. Under macroscale conditions, more materials with superlubricity performance have been studied, including water [23, 93, 94, 131], hydrated materials [47, 53, 54, 60, 168], acid-based solutions [26, 103], polymers [169–173], ILs [51, 52], alkane fluids [174], and 2D materials [65, 149], which were mainly attributed to hydrodynamic lubrication (⬟ in Fig. 10). Hydration lubrication (★ in Fig. 10) significantly contributes to the superlubricity obtained by hydrated materials in both microscale and macroscale conditions. Furthermore, numerical simulations considering the surface force effect (that is hydration force, double-layer force, and van der Waals force) revealed that surface repulsive forces can reduce friction, particularly at mixed lubrication and regime, and a reduction in surface roughness can improve the contribution of short-range surface forces and facilitate the achievement

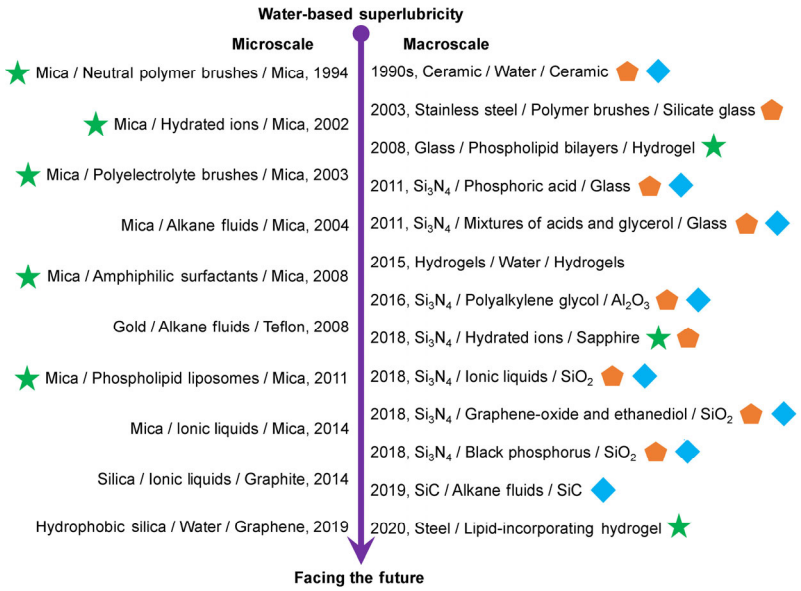

Fig. 10 Timeline of major milestones in research on liquid superlubricity (excluding oil-based superlubricity). Liquid superlubricity can be divided into microscale and macroscale superlubricity according to the contact area and contact pressure. Different symbols represent different mechanisms to achieve superlubricity; ★, ⬟, and ◆ represent hydration effect, hydrodynamic effect, and tribo-induced film or adsorption layer, respectively.

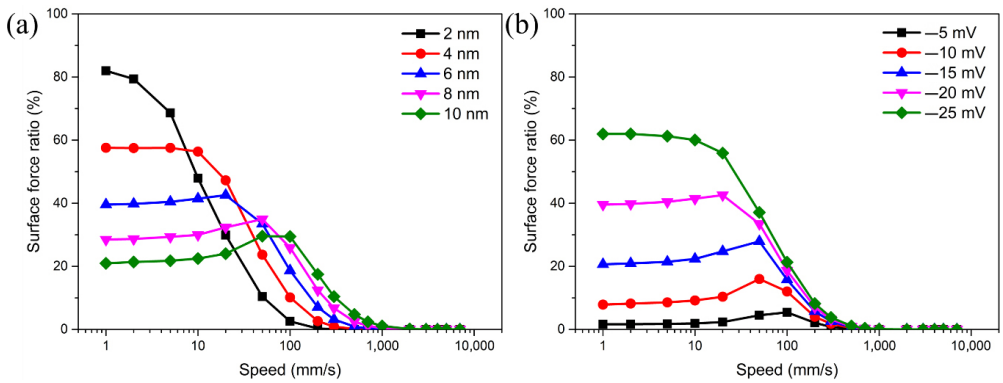

Fig. 11 Ratio of normal load undertaken by surface force at a wide range of sliding speeds obtained using a numerical model where a KCl solution of 0.1 M is taken as the lubricant. Results demonstrate the influence of (a) different root mean square surface roughnesses with a fixed surface potential of −20 mV and (b) different surface potentials with fixed root mean square roughness of 6 nm. The surface potential is related to surface charge density according to the Grahame equation.

of superlubricity at low speeds [136]. Recently, a study by our gruop was conducted and found that for smoother surfaces or more charged materials, the surface forces can bear most of the normal load at the boundary and mixed lubrication regimes (where the hydrodynamic effect is weak); thus, the contact of surface asperities can be separated and the superlubricity can be realized more easily. For a surface with a roughness of 2 nm and surface potential of −20 mV, the contribution of surface forces to bearing the load can be up to 80% (Fig. 11(a)). Generally, the contribution of surface forces increases with a decrease in surface roughness and an increase in surface charge density (Fig. 11). Therefore, strongly charged friction surfaces with low surface roughness may be the basic requirement for future investigations of water-based superlubricity. Moreover, the tribo-induced films or adsorption layers (◆ in Fig. 10) play an important role in the achievement of most macroscale superlubricity at ceramic interfaces along with a tribochemical reaction, which typically has a low shear resistance and can be removed and replenished

during friction [60, 116]. It is usually difficult to characterize the tribofilms *in situ* because they are generated and function at the interfaces; thus, they are evaluated through observations of ultra-low friction and post-test surface analyses (such as XPS, TEM, and ζ-potential analyses) and simulation methods in previous studies [31, 82, 115, 116]. In addition to these superlubricity mechanisms, which can be used to explain most superlubricity phenomena (Fig. 9), other similar mechanisms have been observed in alkane fluids and ILs.

Alkane fluids (such as dodecane, squalene, cyclohexane, and isooctane) exhibit superlubricity under both microscale and macroscale conditions [165–167, 174, 175]. A repulsive van der Waals force was observed in cyclohexane between a gold sphere and a smooth Teflon surface templated on mica, leading to an ultra-low COF of 0.0003 under small loads below 30 nN, which indicates that the alkane fluid retained a low viscosity even for several molecular layers [165, 166, 175]. In addition, significant differences in friction behavior were observed in confined molecular alkane films between two mica surfaces, and an ultra-low COF of 0.001 was observed for a single molecular layer of dodecane trapped between crystallographically misaligned dry surfaces, which was attributed to the sliding of incommensurate solid-like alkane layers [167]. However, superlubricity of isooctane was observed in humid air and dry nitrogen atmosphere between SiC–SiC interfaces at a high load of 200 N, which might result from the hydrodynamic effect and mild wear mechanisms along with the formation of hydroxylated silica gel [174]. Isooctane has a low viscosity of 0.5 mPa·s at 25 °C, which is of the same order of magnitude as that of water; thus, the superlubricity of isooctane between SiC–SiC surfaces is similar to the superlubricity of water between ceramic surfaces. As for ILs, superlubricity can also be achieved under both microscale and macroscale conditions [45, 51, 52, 96, 97]. An ultra-low COF of approximately 0.007 was observed for two bilayers of the ionic liquids ($[C_{10}C_1Pyrr][NTf_2]$) between negatively-charged mica surfaces because the shear occurred along the ionic planes with low shear stress rather than at the alkyl planes for the ionic liquid film with sufficient thickness to contain two or more bilayers [97]. Moreover, the friction of the IL ([HMIm] FAP) was shown to be tunable with positive and negative electric potentials and ion structures at the silica–graphite interface, and the ultra-low COF of approximately 0.001 was obtained at a positive surface potential of 1.5 V [45]. In macroscale conditions, the superlubricity of ILs was attributed to the tribo-induced film (composed of ILs, silica, ammonia-containing compounds, and sulfides), a molecular adsorption layer of ILs, and a fluid layer contributing to hydrodynamic lubrication [51, 52]. It is worth noting that the common feature of superlubricity by alkane fluids and ionic liquids is that the shear plane is transferred from the solid–solid interface into the fluid–fluid interface with a low shear resistance, and remains stable under confinement, which is in good agreement with the origins of hydration lubrication. In summary, most liquid superlubricity phenomena can be explained by the superlubricity mechanism proposed in Fig. 9, that is, both hydrodynamic and separating effects (including hydration effect and tribo-induced boundary films) play key roles in the achievement of superlubricity at the boundary and mixed lubrication regimes. Therefore, the fundamental method to reduce friction is to separate two solid surfaces using low-viscosity fluids with low shear resistances and high load-carrying capacities.

Compared with water-based superlubricity, oil-based superlubricity is challenging in that the repulsion force under a nonaqueous liquid is primarily derived from the hydrodynamic effect, whereas surface forces (including hydration force and electric double layer force) can generate a repulsive force for aqueous solutions. The total COF can be described by the equation $\mu = \mu_f(1 - w_c / w) + \mu_c w_c / w$, where μ_f is the COF of the EHL, μ_c is the COF of the asperity contact region, w is the normal load, and w_c is the normal load supported by asperity contact [176]. Based on a rough prediction, the liquid superlubricity is closely related to the contact pressure and pressure–viscosity coefficient. The higher the contact pressure, the lower the pressure–viscosity coefficient to achieve liquid superlubricity, which makes it difficult to obtain ultra-low COF under high contact pressures because of the high pressure–viscosity coefficient for

oil-based lubricants. Therefore, extending the oil-based superlubricity region to a wide range of velocities and pressures remains a big challenge. According to the thin-film lubrication (TFL) proposed by Luo et al. [102, 177, 178], a new lubrication state describing the transition stage from EHL to BL, TFL with much lower COF (than EHL) can be obtained over a wider velocity range because lubricants have a strong interfacial interaction with friction surfaces and a strong intermolecular interaction. Despite many difficulties, some experimental achievements of oil-based superlubricity have been achieved in the recent past. Thin oil films may lead to superlubricity in the TFL regime under certain conditions. Macroscale superlubricity could be obtained using 1,3-diketone oil with an ultralow COF of 0.005 between steel surfaces under ambient atmosphere [179], which was the first reported oil-based superlubricity obtained through experiments. The superlubricity mechanism of 1,3-diketone oil was mainly attributed to the tribochemical reaction between 1,3-diketone and iron (making the contact surfaces smoother), and 1,3-diketone with a rod-like molecular structure similar to that of liquid crystals (supplying strong intermolecular interactions to form the molecular alignment and reduce shear stress) [79–81, 100]. It is worth noting that the contact pressure during the superlubricity of diketone oil was lower than 20 MPa (< 2 N), and the superlubricity failed at a relatively low sliding speed (< 500 mm/s), which indicated that the hydrodynamic contribution still played an important role in the superlubricity [79, 98]. In addition, superlubricity has been achieved with silicone oil, PAO oil, and castor oil through hydrodynamic contributions between ceramic or nitinol alloy surfaces [56, 83, 84, 86]. In the case of potential industrial applications, the stability and applicability of oil-based superlubricity require further investigation. In addition, more details on oil-based superlubricity can be learned from Ref. [180].

6 Conclusions and outlooks

This review aims to introduce and summarize liquid superlubricity phenomena and unlock the secrets behind these phenomena. To the best of our knowledge, the present study demonstrated the immense progress of this exciting topic since the first theoretical prediction of superlubricity by Hirano and Shinjo et al. [11] in the early 1990s, which provided conclusions on the uniform superlubricity mechanisms at boundary, mixed, and hydrodynamic lubrication regimes (Fig. 9). Systematic analysis of the superlubricity mechanisms provided future research perspectives, encouraging researchers to explore green superlubricating materials and find answers to unresolved problems. Presently, the following problems have not been resolved and are worth studying.

1) How to further improve the contact pressure during superlubricity, that is, how can the load-carrying capacity of lubricants be further enhanced? For biological applications such as artificial joints, hydration lubrication provides a good solution to reduce friction because the contact pressures between cartilage surfaces are 10–20 MPa [181, 182]. For engineering applications such as bearings and gears, higher contact pressures, even above 1 GPa, are required [6, 183]. To date, the maximum average contact pressure to achieve liquid superlubricity is approximately 500–600 MPa, which is based on mixtures of GO nanosheets and ILs, mixtures of hydrated ions and polyethylene glycol solutions, and mixtures of hydrated ions and poly(vinyl alcohol) solutions [60, 64, 137]. The achievement of superlubricity under extremely high pressures of above 1 GPa is still far-fetched.

2) How can liquid superlubricity be obtained without a running-in period under high contact pressures (typically up to 100 MPa)? Thus far, a long running-in stage exists in almost all superlubricity systems, which causes serious wear of friction materials. Although the running-in time decreased to less than 1 min by combining hydration and hydrodynamic contributions, the wear of solid surfaces was still present [60]. There is no need to consider wear problems if one day the superlubricity can be obtained directly without a running-in period; thus, the service life of materials and equipment will be significantly improved.

3) Oil-based superlubricity is a potential direction for superlubricity with future technological implications because lubricating oils and greases are still the most widely used lubricants in practical mechanical systems. However, owing to their high

viscosity (at least two orders of magnitude higher than that of water), the minimum COF of conventional oil-based lubricants is typically approximately 0.01–0.05. According to the calculation based on the Hamrock–Dowson theory for EHL regimes, the realization of liquid superlubricity depends on the pressure–viscosity coefficient and contact pressure [56, 58]. Under high pressures, superlubricity can only be achieved when the lubricating oil has a low pressure–viscosity coefficient; however, the challenge is that a high load-carrying capacity and a low pressure–viscosity coefficient are usually mutually exclusive. To date, significant progress has been made in oil-based superlubricity, and some lubricating oils have exhibited excellent lubrication performance under contact pressures below 100 MPa. A macroscopic ultra-low COF of 0.005 can be obtained using 1,3-diketone on steel surfaces under an ambient atmosphere in the TFL regime, which was attributed to the tribochemical reaction between 1,3-diketone and iron, a strong adsorbed layer formed on steel surfaces via chemical bonds, and molecular alignment of 1,3-diketone formed owing to strong intermolecular interactions with low shear stress [79–81, 98, 100]. In addition, other lubricating oils, including silicone oil, PAO oil, castor oil, and oleic acid exhibit superlubricity characteristics between Si_3N_4–DLC, Si_3N_4–glass, stell–DLC, nitinol 60 alloy–steel, steel–steel interfaces, mainly resulting from the hydrodynamic effect and tribo-induced boundary films [83, 84, 86, 99, 184]. Therefore, oil-based superlubricity can also be explained using the mechanisms proposed in Fig. 9; that is, based on the hydrodynamic and separating effects such as tribo-induced boundary films, water-based lubricants are more suitable for corrosion-resistant ceramic and polymer surfaces; however, oil-based lubricants can be used for steel surfaces and are expected to be employed in most existing application environments and operating conditions. Furthermore, modified graphene is a novel lubricating additive with high dispersion stability in oil; thus, it is expected to obtain oil-based superlubricity with 2D materials as additives in the near future [85, 185].

4) Liquid superlubricity has recently been focused on identifying systems those exhibit the following key features: smooth surfaces (< 10 nm), liquids with low viscosity and low pressure–viscosity coefficient (like water), high load-carrying capacity, and low shear resistance. For smooth surfaces, mica, graphite, ceramics, and steels after the running-in period are all commonly used friction surfaces. However, conventional engineering components are likely to be rough (approximately 1 μm), which is much higher than the surface roughness used in experimental studies [186]. For liquids with low viscosity and low pressure–viscosity coefficient, conventional engineering components are usually lubricated with oil, which is much more viscous than aqueous lubricants. Moreover, lubricating additives are almost always needed in the oil to perform specific functions (such as oxidation resistance, rust prevention, and heat dissipation) in the lubricant; thus, more attention should be paid to liquid superlubricity considering lubricating additives. Presently, novel ideas should be applied to resolve the load support–low shear conflict in idealized cases to more widely relevant application conditions. Except for hydration lubrication and 2D materials, new superlubricity mechanisms should be studied, especially tribochemical reactions between lubricants and friction surfaces. The exploration of novel liquid superlubricity mechanisms should never stop; that is, identifying and extending superlubricity mechanisms under a wider range of conditions (including high pressures and low velocity) is a significant direction for future research, which may have an important impact on engineering applications.

5) How can the superlubricity technique be applied to technological applications? The final foothold of all technologies is application; otherwise, it can only be unrealistic goals [187]. In the case of potential biological and industrial applications, the stability and applicability of liquid superlubricity require further investigation. It is expected that macroscale superlubricity in an ambient atmosphere and in a vacuum over a wide range of operating conditions. Water-based superlubricity is expected to be effective in biological fields such as artificial joints and water lubrication systems, such as ceramic bearings. Oil-based superlubricity has important practical applications in common systems, such as automobile engines. It is firmly believed that the fundamental theoretical and experimental studies, as well as the

research, focused on extending the application ranges of technological developments will coexist and promote each other for a long time, enabling a sustainable state of ultra-low friction and ultra-low wear and transformative improvements in the efficiency of mechanical systems [68, 188].

Acknowledgements

This work is financially supported by the National Key R&D Program of China (No. 2018YFB2002204) and the National Natural Science Foundation of China (No. 51925506). Tianyi HAN gratefully acknowledges the financial support from the non-profit China Scholarship Council, China. We thank Prof. Xavier Banquy, working at the Faculty of Pharmacy, University of Montreal, Canada, for useful discussions.

References

[1] Holmberg K, Andersson P, Erdemir A. Global energy consumption due to friction in passenger cars. *Tribol Int* **47**: 221–234 (2012)

[2] Holmberg K, Erdemir A. The impact of tribology on energy use and CO_2 emission globally and in combustion engine and electric cars. *Tribol Int* **135**: 389–396 (2019)

[3] Holmberg K, Erdemir A. Influence of tribology on global energy consumption, costs and emissions. *Friction* **5**(3): 263–284 (2017)

[4] Wang H D, Xu B S, Liu J J. *Micro and Nano Sulfide Solid Lubrication*. Beijing (China): Science Press Beijing & Springer, 2012.

[5] Luo J B. Investigation on the origin of friction and superlubricity. *Chinese Sci Bull* **65**(27): 2966–2978 (2020) (in Chinese)

[6] Kato K. Industrial tribology in the past and future. *Tribol Online* **6**(1): 1–9 (2011)

[7] Peter Jost H, Schofield J. Energy saving through tribology: A techno-economic study. *Proc Inst Mech Eng* **195**(1): 151–173 (1981)

[8] Dowson D. *History of tribology*. Chichester (UK): Wiley, 1998.

[9] Shinjo K, Hirano M. Dynamics of friction: Superlubric state. *Surf Sci* **283**(1–3): 473–478 (1993)

[10] Hirano M, Shinjo K. Superlubricity and frictional anisotropy. *Wear* **168**(1–2): 121–125 (1993)

[11] Hirano M, Shinjo K, Kaneko R, Murata Y. Anisotropy of frictional forces in muscovite mica. *Phys Rev Lett* **67**(19): 2642–2645 (1991)

[12] Hirano M, Shinjo K, Kaneko R, Murata Y. Observation of superlubricity by scanning tunneling microscopy. *Phys Rev Lett* **78**(8): 1448–1451 (1997)

[13] Zhai W Z, Zhou K. Nanomaterials in superlubricity. *Adv Funct Mater* **29**(28): 1806395 (2019)

[14] Dienwiebel M, Verhoeven G S, Pradeep N, Frenken J W M, Heimberg J A, Zandbergen H W. Superlubricity of graphite. *Phys Rev Lett* **92**(12): 126101 (2004)

[15] Vu C C, Zhang S M, Urbakh M, Li Q Y, He Q C, Zheng Q S. Observation of normal-force-independent superlubricity in mesoscopic graphite contacts. *Phys Rev B* **94**: 081405(R) (2016)

[16] Erdemir A, Eryilmaz O L, Fenske G. Synthesis of diamondlike carbon films with superlow friction and wear properties. *J Vac Sci Technol A* **18**(4): 1987–1992 (2000)

[17] Chen X C, Kato T, Nosaka M. Origin of superlubricity in a-C:H:Si films: A relation to film bonding structure and environmental molecular characteristic. *ACS Appl Mater Interfaces* **6**(16): 13389–13405 (2014)

[18] Cumings J, Zettl A. Low-friction nanoscale linear bearing realized from multiwall carbon nanotubes. *Science* **289**(5479): 602–604 (2000)

[19] Martin J M, Donnet C, Mogne T L, Epicier T. Superlubricity of molybdenum disulphide. *Phys Rev B Condens Matter* **48**(14): 10583–10586 (1993)

[20] Berman D, Deshmukh S A, Sankaranarayanan S K R S, Erdemir A, Sumant A V. Friction. Macroscale superlubricity enabled by graphene nanoscroll formation. *Science* **348**(6239): 1118–1122 (2015)

[21] Liu Y M, Song A S, Xu Z, Zong R L, Zhang J, Yang W Y, Wang R, Hu Y Z, Luo J B, Ma T B. Interlayer friction and superlubricity in single-crystalline contact enabled by two-dimensional flake-wrapped atomic force microscope tips. *ACS Nano* **12**(8): 7638–7646 (2018)

[22] Berman D, Erdemir A, Sumant A V. Approaches for achieving superlubricity in two-dimensional materials. *ACS Nano* **12**(3): 2122–2137 (2018)

[23] Tomizawa H, Fischer T E. Friction and wear of silicon nitride and silicon carbide in water: Hydrodynamic lubrication at low sliding speed obtained by tribochemical wear. *ASLE Trans* **30**(1): 41–46 (1987)

[24] Wong H, Umehara N, Kato K. The effect of surface roughness on friction of ceramics sliding in water. *Wear* **218**(2): 237–243 (1998)

[25] Chen M, Kato K, Adachi K. Friction and wear of self-mated SiC and Si_3N_4 sliding in water. *Wear* **250**(1–12): 246–255 (2001)

[26] Li J J, Zhang C H, Luo J B. Superlubricity behavior with phosphoric acid-water network induced by rubbing. *Langmuir* **27**(15): 9413–9417 (2011)

[27] Deng M M, Zhang C H, Li J J, Ma L R, Luo J B. Hydrodynamic effect on the superlubricity of phosphoric acid between ceramic and sapphire. *Friction* **2**(2): 173–181 (2014)

[28] Li J J, Zhang C H, Deng M M, Luo J B. Investigations of the superlubricity of sapphire against ruby under phosphoric acid lubrication. *Friction* **2**(2): 164–172 (2014)

[29] Li J J, Zhang C H, Ma L R, Liu Y H, Luo J B. Superlubricity achieved with mixtures of acids and glycerol. *Langmuir* **29**(1): 271–275 (2013)

[30] Li J J, Zhang C H, Luo J B. Superlubricity achieved with mixtures of polyhydroxy alcohols and acids. *Langmuir* **29**(17): 5239–5245 (2013)

[31] Deng M M, Li J J, Zhang C H, Ren J, Zhou N N, Luo J B. Investigation of running-in process in water-based lubrication aimed at achieving super-low friction. *Tribol Int* **102**: 257–264 (2016)

[32] Raviv U, Klein J. Fluidity of bound hydration layers. *Science* **297**(5586): 1540–1543 (2002)

[33] Ma L R, Gaisinskaya-Kipnis A, Kampf N, Klein J. Origins of hydration lubrication. *Nat Commun* **6**: 6060 (2015)

[34] Klein J, Kumacheva E, Mahalu D, Perahia D, Fetters L J. Reduction of frictional forces between solid surfaces bearing polymer brushes. *Nature* **370**(6491): 634–636 (1994)

[35] Raviv U, Giasson S, Kampf N, Gohy J F, Jérôme R, Klein J. Lubrication by charged polymers. *Nature* **425**(6954): 163–165 (2003)

[36] Briscoe W H, Titmuss S, Tiberg F, Thomas R K, McGillivray D J, Klein J. Boundary lubrication under water. *Nature* **444**(7116): 191–194 (2006)

[37] Goldberg R, Schroeder A, Silbert G, Turjeman K, Barenholz Y, Klein J. Boundary lubricants with exceptionally low friction coefficients based on 2D close-packed phosphatidylcholine liposomes. *Adv Mater* **23**(31): 3517–3521 (2011)

[38] Sorkin R, Kampf N, Zhu L, Klein J. Hydration lubrication and shear-induced self-healing of lipid bilayer boundary lubricants in phosphatidylcholine dispersions. *Soft Matter* **12**(10): 2773–2784 (2016)

[39] Kang T, Banquy X, Heo J, Lim C, Lynd N A, Lundberg P, Oh D X, Lee H K, Hong Y K, Hwang D S, et al. Mussel-inspired anchoring of polymer loops that provide superior surface lubrication and antifouling properties. *ACS Nano* **10**(1): 930–937 (2016)

[40] Banquy X, Burdyńska J, Lee D W, Matyjaszewski K, Israelachvili J. Bioinspired bottle-brush polymer exhibits low friction and amontons-like behavior. *J Am Chem Soc* **136**(17): 6199–6202 (2014)

[41] Cao Y, Kampf N, Klein J. Boundary lubrication, hemifusion, and self-healing of binary saturated and monounsaturated phosphatidylcholine mixtures. *Langmuir* **35**(48): 15459–15468 (2019)

[42] Cao Y F, Kampf N, Lin W F, Klein J. Normal and shear forces between boundary sphingomyelin layers under aqueous conditions. *Soft Matter* **16**(16): 3973–3980 (2020)

[43] Adibnia V, Ma Y S, Halimi I, Walker G C, Banquy X, Kumacheva E. Phytoglycogen nanoparticles: Nature-derived superlubricants. *ACS Nano* **15**(5): 8953–8964 (2021)

[44] Perkin S, Albrecht T, Klein J. Layering and shear properties of an ionic liquid, 1-ethyl-3-methylimidazolium ethylsulfate, confined to nano-films between mica surfaces. *Phys Chem Chem Phys* **12**(6): 1243–1247 (2010)

[45] Li H, Wood R J, Rutland M W, Atkin R. An ionic liquid lubricant enables superlubricity to be "switched on" *in situ* using an electrical potential. *Chem Commun* **50**(33): 4368–4370 (2014)

[46] Nomura A, Ohno K, Fukuda T, Sato T, Tsujii Y. Lubrication mechanism of concentrated polymer brushes in solvents: Effect of solvent viscosity. *Polym Chem* **3**(1): 148–153 (2012)

[47] Müller M, Lee S, Spikes H A, Spencer N D. The influence of molecular architecture on the macroscopic lubrication properties of the brush-like co-polyelectrolyte poly(L-lysine)-*g*-poly(ethylene glycol) (PLL-*g*-PEG) adsorbed on oxide surfaces. *Tribol Lett* **15**(4): 395–405 (2003)

[48] Hartung W, Rossi A, Lee S, Spencer N D. Aqueous lubrication of SiC and Si_3N_4 ceramics aided by a brush-like copolymer additive, poly(L-lysine)-*graft*-poly(ethylene glycol). *Tribol Lett* **34**(3): 201–210 (2009)

[49] Wang Z N, Li J J, Jiang L, Xiao S, Liu Y H, Luo J B. Zwitterionic hydrogel incorporated graphene oxide nanosheets with improved strength and lubricity. *Langmuir* **35**(35): 11452–11462 (2019)

[50] Wang Z N, Li J J, Liu Y H, Luo J B. Macroscale superlubricity achieved between zwitterionic copolymer hydrogel and sapphire in water. *Mater Des* **188**: 108441 (2020)

[51] Ge X Y, Li J J, Zhang C H, Wang Z N, Luo J B. Superlubricity of 1-ethyl-3-methylimidazolium trifluoromethanesulfonate ionic liquid induced by tribochemical reactions. *Langmuir* **34**(18): 5245–5252 (2018)

[52] Ge X Y, Li J J, Zhang C H, Liu Y H, Luo J B. Superlubricity and antiwear properties of in situ-formed ionic liquids at ceramic interfaces induced by tribochemical reactions. *ACS Appl Mater Interfaces* **11**(6): 6568–6574 (2019)

[53] Han T Y, Zhang C H, Luo J B. Macroscale superlubricity enabled by hydrated alkali metal ions. *Langmuir* **34**(38): 11281–11291 (2018)

[54] Han T Y, Zhang C H, Li J J, Yuan S H, Chen X C, Zhang J Y, Luo J B. Origins of superlubricity promoted by hydrated multivalent ions. *J Phys Chem Lett* **11**(1): 184–190 (2020)

[55] Ma W, Gong Z B, Gao K X, Qiang L, Zhang J Y, Yu S R. Superlubricity achieved by carbon quantum dots in ionic liquid. *Mater Lett* **195**: 220–223 (2017)

[56] Li J J, Zhang C H, Deng M M, Luo J B. Investigation of the difference in liquid superlubricity between water- and oil-based lubricants. *RSC Adv* **5**(78): 63827–63833 (2015)

[57] Erdemir A, Martin J M. *Superlubricity*. Amsterdam (the Netherlands): Elsevier B.V., 2007.

[58] Zhang C H, Li K, Luo J B. Superlubricity with nonaqueous liquid. In *Superlubricity*. 2nd edn. Erdemir A, Martin J M, Luo J B, Eds. Amsterdam (the Netherlands): Elsevier B.V., 2021: 379–403.

[59] Jia W P, Tian J M, Bai P P, Li S W, Zeng H B, Zhang W L, Tian Y. A novel comb-typed poly(oligo(ethylene glycol) methylether acrylate) as an excellent aqueous lubricant. *J Colloid Interface Sci* **539**: 342–350 (2019)

[60] Han T Y, Yi S, Zhang C H, Li J J, Chen X C, Luo J B, Banquy X. Superlubrication obtained with mixtures of hydrated ions and polyethylene glycol solutions in the mixed and hydrodynamic lubrication regimes. *J Colloid Interface Sci* **579**: 479–488 (2020)

[61] Liu L C, Zhou M, Li X, Jin L, Su G S, Mo Y T, Li L C, Zhu H W, Tian Y. Research progress in application of 2D materials in liquid-phase lubrication system. *Materials* **11**(8): 1314 (2018)

[62] Luo J B, Liu M, Ma L R. Origin of friction and the new frictionless technology—Superlubricity: Advancements and future outlook. *Nano Energy* **86**: 106092 (2021)

[63] Liu L C, Zhou M, Jin L, Li L C, Mo Y T, Su G S, Li X, Zhu H W, Tian Y. Recent advances in friction and lubrication of graphene and other 2D materials: Mechanisms and applications. *Friction* **7**(3): 199–216 (2019)

[64] Ge X Y, Li J J, Wang H D, Zhang C H, Liu Y H, Luo J B. Macroscale superlubricity under extreme pressure enabled by the combination of graphene-oxide nanosheets with ionic liquid. *Carbon* **151**: 76–83 (2019)

[65] Wang W, Xie G X, Luo J B. Superlubricity of black phosphorus as lubricant additive. *ACS Appl Mater Interfaces* **10**(49): 43203–43210 (2018)

[66] Wu S, He F, Xie G X, Bian Z L, Luo J B, Wen S Z. Black phosphorus: Degradation favors lubrication. *Nano Lett* **18**(9): 5618–5627 (2018)

[67] Wu S, He F, Xie G, Bian Z, Ren Y, Liu X, Yang H, Guo D, Zhang L, Wen S, et al. Super-slippery degraded black phosphorus/silicon dioxide interface. *ACS Appl Mater Interfaces* **12**(6): 7717–7726 (2020)

[68] Baykara M Z, Vazirisereshk M R, Martini A. Emerging superlubricity: A review of the state of the art and perspectives on future research. *Appl Phys Rev* **5**(4): 041102 (2018)

[69] Leng Y S, Cummings P T. Hydration structure of water confined between mica surfaces. *J Chem Phys* **124**(7): 074711 (2006)

[70] Leng Y S, Cummings P T. Fluidity of hydration layers nanoconfined between mica surfaces. *Phys Rev Lett* **94**(2): 026101 (2005)

[71] Christenson H K, Thomson N H. The nature of the air-cleaved mica surface. *Surf Sci Rep* **71**(2): 367–390 (2016)

[72] Leng Y S. Hydration force between mica surfaces in aqueous KCl electrolyte solution. *Langmuir* **28**(12): 5339–5349 (2012)

[73] Ricci M, Spijker P, Voïtchovsky K. Water-induced correlation between single ions imaged at the solid–liquid interface. *Nat Commun* **5**: 4400 (2014)

[74] Qiu Y H, Ma J, Chen Y F. Ionic behavior in highly concentrated aqueous solutions nanoconfined between discretely charged silicon surfaces. *Langmuir* **32**(19): 4806–4814 (2016)

[75] Nishimura S, Tateyama H, Tsunematsu K, Jinnai K. Zeta potential measurement of muscovite mica basal plane-aqueous

solution interface by means of plane interface technique. *J Colloid Interface Sci* **152**(2): 359–367 (1992)

[76] Li J J, Cao W, Li J F, Ma M, Luo J B. Molecular origin of superlubricity between graphene and a highly hydrophobic surface in water. *J Phys Chem Lett* **10**(11): 2978–2984 (2019)

[77] Li J J, Cao W, Wang Z N, Ma M, Luo J B. Origin of hydration lubrication of zwitterions on graphene. *Nanoscale* **10**(35): 16887–16894 (2018)

[78] Sugahara A, Ando Y, Kajiyama S, Yazawa K, Gotoh K, Otani M, Okubo M, Yamada A. Negative dielectric constant of water confined in nanosheets. *Nat Commun* **10**: 850 (2019)

[79] Zhang S M, Zhang C H, Chen X C, Li K, Jiang J M, Yuan C Q, Luo J B. XPS and ToF-SIMS analysis of the tribochemical absorbed films on steel surfaces lubricated with diketone. *Tribol Int* **130**: 184–190 (2019)

[80] Li K, Zhang S M, Liu D S, Amann T, Zhang C H, Yuan C Q, Luo J B. Superlubricity of 1,3-diketone based on autonomous viscosity control at various velocities. *Tribol Int* **126**: 127–132 (2018)

[81] Li K, Amann T, Walter M, Moseler M, Kailer A, Rühe J. Ultralow friction induced by tribochemical reactions: A novel mechanism of lubrication on steel surfaces. *Langmuir* **29**(17): 5207–5213 (2013)

[82] Liu Y F, Li J J, Ge X Y, Yi S, Wang H D, Liu Y H, Luo J B. Macroscale superlubricity achieved on the hydrophobic graphene coating with glycerol. *ACS Appl Mater Interfaces* **12**(16): 18859–18869 (2020)

[83] Zeng Q F, Yu F, Dong G N. Superlubricity behaviors of Si_3N_4/DLC films under PAO oil with nano boron nitride additive lubrication. *Surf Interface Anal* **45**(8): 1283–1290 (2013)

[84] Zeng Q F, Dong G N, Martin J M. Green superlubricity of Nitinol 60 alloy against steel in presence of castor oil. *Sci Rep* **6**: 29992 (2016)

[85] Wu P, Chen X C, Zhang C H, Zhang J P, Luo J B, Zhang J Y. Modified graphene as novel lubricating additive with high dispersion stability in oil. *Friction* **9**(1): 143–154 (2021)

[86] Ge X Y, Halmans T, Li J J, Luo J B. Molecular behaviors in thin film lubrication—Part three: Superlubricity attained by polar and nonpolar molecules. *Friction* **7**(6): 625–636 (2019)

[87] Sorkin R, Dror Y, Kampf N, Klein J. Mechanical stability and lubrication by phosphatidylcholine boundary layers in the vesicular and in the extended lamellar phases. *Langmuir* **30**(17): 5005–5014 (2014)

[88] Sorkin R, Kampf N, Dror Y, Shimoni E, Klein J. Origins of extreme boundary lubrication by phosphatidylcholine liposomes. *Biomaterials* **34**(22): 5465–5475 (2013)

[89] Chen M, Briscoe W H, Armes S P, Klein J. Lubrication at physiological pressures by polyzwitterionic brushes. *Science* **323**(5922): 1698–1701 (2009)

[90] Li J J, Zhang C H, Cheng P, Chen X C, Wang W Q, Luo J B. AFM studies on liquid superlubricity between silica surfaces achieved with surfactant micelles. *Langmuir* **32**(22): 5593–5599 (2016)

[91] Kampf N, Wu C X, Wang Y L, Klein J. A trimeric surfactant: Surface micelles, hydration–lubrication, and formation of a stable, charged hydrophobic monolayer. *Langmuir* **32**(45): 11754–11762 (2016)

[92] Pitenis A A, Urueña J M, Schulze K D, Nixon R M, Dunn A C, Krick B A, Sawyer W G, Angelini T E. Polymer fluctuation lubrication in hydrogel gemini interfaces. *Soft Matter* **10**(44): 8955–8962 (2014)

[93] Urueña J M, Pitenis A A, Nixon R M, Schulze K D, Angelini T E, Sawyer W G. Mesh size control of polymer fluctuation lubrication in gemini hydrogels. *Biotribology* **1–2**: 24–29 (2015)

[94] Pitenis A A, Manuel Urueña J, Cooper A C, Angelini T E, Sawyer W G. Superlubricity in gemini hydrogels. *J Tribol* **138**(4): 042103 (2016)

[95] Lin W F, Kluzek M, Iuster N, Shimoni E, Kampf N, Goldberg R, Klein J. Cartilage-inspired, lipid-based boundary-lubricated hydrogels. *Science* **370**(6514): 335–338 (2020)

[96] Lhermerout R, Perkin S. A new methodology for a detailed investigation of quantized friction in ionic liquids. *Phys Chem Chem Phys* **22**(2): 455–466 (2020)

[97] Smith A M, Parkes M A, Perkin S. Molecular friction mechanisms across nanofilms of a bilayer-forming ionic liquid. *J Phys Chem Lett* **5**(22): 4032–4037 (2014)

[98] Zhang S M, Zhang C H, Li K, Luo J B. Investigation of ultra-low friction on steel surfaces with diketone lubricants. *RSC Adv* **8**(17): 9402–9408 (2018)

[99] Li J J, Zhang C H, Deng M M, Luo J B. Superlubricity of silicone oil achieved between two surfaces by running-in with acid solution. *RSC Adv* **5**(39): 30861–30868 (2015)

[100] Li K, Amann T, List M, Walter M, Moseler M, Kailer A, Rühe J. Ultralow friction of steel surfaces using a 1,3-diketone lubricant in the thin film lubrication regime. *Langmuir* **31**(40): 11033–11039 (2015)

[101] Arad SM, Rapoport L, Moshkovich A, van Moppes D, Karpasas M, Golan R, Golan Y. Superior biolubricant from a species of red microalga. *Langmuir* **22**(17): 7313–7317 (2006)

[102] Luo J B, Lu X C, Wen S Z. Developments and unsolved problems in nano-lubrication. *Prog Nat Sci* **11**(3): 173–183 (2001)

[103] Zhang C H, Ma Z Z, Luo J B, Lu X C, Wen S Z. Superlubricity of a mixed aqueous solution. *Chin Phys Lett* **28**(5): 056201 (2011)

[104] Zhang S H, Qiao Y J, Liu Y H, Ma L R, Luo J B. Molecular behaviors in thin film lubrication—Part one: Film formation for different polarities of molecules. *Friction* **7**(4): 372–387 (2019)

[105] Ma L R, Luo J B, Zhang C H, Ma Z Z, Wang Y, Dai Y J. Film formation of yogurt under confined condition. *Surf Interface Anal* **44**(2): 258–262 (2012)

[106] Li J J, Ma L R, Zhang S H, Zhang C H, Liu Y H, Luo J B. Investigations on the mechanism of superlubricity achieved with phosphoric acid solution by direct observation. *J Appl Phys* **114**(11): 114901 (2013)

[107] Sun L, Zhang C H, Li J J, Liu Y H, Luo J B. Superlubricity of Si_3N_4 sliding against SiO_2 under linear contact conditions in phosphoric acid solutions. *Sci China Technol Sci* **56**(7): 1678–1684 (2013)

[108] Ge X Y, Li J J, Zhang C H, Luo J B. Liquid superlubricity of polyethylene glycol aqueous solution achieved with boric acid additive. *Langmuir* **34**(12): 3578–3587 (2018)

[109] Li J J, Zhang C H, Sun L, Lu X C, Luo J B. Tribochemistry and superlubricity induced by hydrogen ions. *Langmuir* **28**(45): 15816–15823 (2012)

[110] Gao Y, Ma L R, Liang Y, Li B H, Luo J B. Water molecules on the liquid superlubricity interfaces achieved by phosphoric acid solution. *Biosurface and Biotribology* **4**(3): 94–98 (2018)

[111] Ge X Y, Li J J, Luo J B. Macroscale superlubricity achieved with various liquid molecules: A review. *Front Mech Eng* **5**: 2 (2019)

[112] Xiao C, Li J J, Gong J, Chen L, Zhang J Y, Qian L M, Luo J B. Gradual degeneration of liquid superlubricity: Transition from superlubricity to ordinary lubrication, and lubrication failure. *Tribol Int* **130**: 352–358 (2019)

[113] Ma L R, Zhang C H. Discussion on the technique of relative optical interference intensity for the measurement of lubricant film thickness. *Tribol Lett* **36**(3): 239–245 (2009)

[114] Wen S Z, Huang P. *Principles of Tribology*. 2nd edn. Beijing (China): Tsinghua University Press, 2017.

[115] Han T Y, Zhang C H, Chen X C, Li J J, Wang W Q, Luo J B. Contribution of a tribo-induced silica layer to macroscale superlubricity of hydrated ions. *J Phys Chem C* **123**(33): 20270–20277 (2019)

[116] Ootani Y, Xu J X, Takahashi N, Akagami K, Sakaki S, Wang Y, Ozawa N, Hatano T, Adachi K, Kubo M. Self-formed double tribolayers play collaborative roles in achieving superlow friction in an aqueous environment. *J Phys Chem C* **124**(15): 8295–8303 (2020)

[117] Xiao C, Li J J, Chen L, Zhang C H, Zhou N N, Qing T, Qian L M, Zhang J Y, Luo J B. Water-based superlubricity in vacuum. *Friction* **7**(2): 192–198 (2019)

[118] Zhao F, Li H X, Ji L, Mo Y F, Quan W L, Du W, Zhou H D, Chen J M. Superlow friction behavior of Si-doped hydrogenated amorphous carbon film in water environment. *Surf Coat Technol* **203**(8): 981–985 (2009)

[119] Ma L R, Zhang C H, Liu S H. Progress in experimental study of aqueous lubrication. *Chin Sci Bull* **57**(17): 2062–2069 (2012)

[120] Tadokoro C, Nihira T, Nakano K. Minimization of friction at various speeds using autonomous viscosity control of nematic liquid crystal. *Tribol Lett* **56**(2): 239–247 (2014)

[121] Lee S H, Müller M, Ratoi-Salagean M, Vörös J, Pasche S, Paul S M D, Spikes H A, Textor M, Spencer N D. Boundary lubrication of oxide surfaces by poly(L-lysine)-*g*-poly(ethylene glycol) (PLL-*g*-PEG) in aqueous media. *Tribol Lett* **15**(3): 231–239 (2003)

[122] Israelachvili J N, Pashley R M. Molecular layering of water at surfaces and origin of repulsive hydration forces. *Nature* **306**(5940): 249–250 (1983)

[123] Goldberg R, Chai L, Perkin S, Kampf N, Klein J. Breakdown of hydration repulsion between charged surfaces in aqueous Cs^+ solutions. *Phys Chem Chem Phys* **10**(32): 4939 (2008)

[124] Perkin S, Goldberg R, Chai L, Kampf N, Klein J. Dynamic properties of confined hydration layers. *Faraday Discuss* **141**: 399–413 (2009)

[125] Gaisinskaya A, Ma L R, Silbert G, Sorkin R, Tairy O, Goldberg R, Kampf N, Klein J. Hydration lubrication: Exploring a new paradigm. *Faraday Discuss* **156**: 217–233 (2012)

[126] Raviv U, Laurat P, Klein J. Fluidity of water confined to subnanometre films. *Nature* **413**(6851): 51–54 (2001)

[127] Klein J. Hydration lubrication. *Friction* **1**(1): 1–23 (2013)

[128] Jahn S, Klein J. Hydration lubrication: The macromolecular domain. *Macromolecules* **48**(15): 5059–5075 (2015)

[129] Rosenhek-Goldian I, Kampf N, Klein J. Trapped aqueous films lubricate highly hydrophobic surfaces. *ACS Nano* **12**(10): 10075–10083 (2018)

[130] Gaisinskaya-Kipnis A, Ma L R, Kampf N, Klein J. Frictional dissipation pathways mediated by hydrated alkali metal ions. *Langmuir* **32**(19): 4755–4764 (2016)

[131] Chen M, Katô K, Adachi K. The difference in running-in period and friction coefficient between self-mated Si_3N_4 and SiC under water lubrication. *Tribol Lett* **11**(1): 23–28 (2001)

[132] Xu J G, Kato K, Hirayama T. The transition of wear mode during the running-in process of silicon nitride sliding in water. *Wear* **205**(1–2): 55–63 (1997)

[133] Garrec D A, Norton I T. Boundary lubrication by sodium salts: A Hofmeister series effect. *J Colloid Interface Sci* **379**(1): 33–40 (2012)

[134] Pashley R M. Forces between mica surfaces in La^{3+} and Cr^{3+} electrolyte solutions. *J Colloid Interface Sci* **102**(1): 23–35 (1984)

[135] Pashley R M, Israelachvili J N. Dlvo and hydration forces between mica surfaces in Mg^{2+}, Ca^{2+}, Sr^{2+}, and Ba^{2+} chloride solutions. *J Colloid Interface Sci* **97**(2): 446–455 (1984)

[136] Zhang S W, Zhang C H, Hu Y Z, Ma L R. Numerical simulation of mixed lubrication considering surface forces. *Tribol Int* **140**: 105878 (2019)

[137] Li S W, Bai P P, Li Y Z, Jia W P, Li X X, Meng Y G, Ma L R, Tian Y. Extreme-pressure superlubricity of polymer solution enhanced with hydrated salt ions. *Langmuir* **36**(24): 6765–6774 (2020)

[138] Chai L, Goldberg R, Kampf N, Klein J. Selective adsorption of poly(ethylene oxide) onto a charged surface mediated by alkali metal ions. *Langmuir* **24**(4): 1570–1576 (2008)

[139] Yuan S H, Chen X C, Zhang C H. Reducing friction by control of isoelectric point: A potential method to design artificial cartilage. *Adv Mater Interfaces* **7**(15): 2000485 (2020)

[140] Yuan H Y, Liu G M. Ionic effects on synthetic polymers: From solutions to brushes and gels. *Soft Matter* **16**(17): 4087–4104 (2020)

[141] Yu J, Jackson N E, Xu X, Morgenstern Y, Kaufman Y, Ruths M, de Pablo J J, Tirrell M. Multivalent counterions diminish the lubricity of polyelectrolyte brushes. *Science* **360**(6396): 1434–1438 (2018)

[142] Brettmann B, Pincus P, Tirrell M. Lateral structure formation in polyelectrolyte brushes induced by multivalent ions. *Macromolecules* **50**(3): 1225–1235 (2017)

[143] Adibnia V, Olszewski M, de Crescenzo G, Matyjaszewski K, Banquy X. Superlubricity of zwitterionic bottlebrush polymers in the presence of multivalent ions. *J Am Chem Soc* **142**(35): 14843–14847 (2020)

[144] Wei Q B, Pei X W, Hao J Y, Cai M R, Zhou F, Liu W M. Surface modification of diamond-like carbon film with polymer brushes using a bio-inspired catechol anchor for excellent biological lubrication. *Adv Mater Interfaces* **1**(5): 1400035 (2014)

[145] Wei Q B, Cai M R, Zhou F, Liu W M. Dramatically tuning friction using responsive polyelectrolyte brushes. *Macromolecules* **46**(23): 9368–9379 (2013)

[146] Lin W F, Kampf N, Goldberg R, Driver M J, Klein J. Poly-phosphocholinated liposomes form stable superlubrication vectors. *Langmuir* **35**(18): 6048–6054 (2019)

[147] Lin W F, Kampf N, Klein J. Designer nanoparticles as robust superlubrication vectors. *ACS Nano* **14**(6): 7008–7017 (2020)

[148] Hod O, Meyer E, Zheng Q S, Urbakh M. Structural superlubricity and ultralow friction across the length scales. *Nature* **563**(7732): 485–492 (2018)

[149] Ge X Y, Li J J, Luo R, Zhang C H, Luo J B. Macroscale superlubricity enabled by the synergy effect of graphene-oxide nanoflakes and ethanediol. *ACS Appl Mater Interfaces* **10**(47): 40863–40870 (2018)

[150] Sinclair R C, Suter J L, Coveney P V. Graphene–graphene interactions: Friction, superlubricity, and exfoliation. *Adv Mater* **30**(13): 1705791 (2018)

[151] Wu P, Li X M, Zhang C H, Chen X C, Lin S Y, Sun H Y, Lin C T, Zhu H W, Luo J B. Self-assembled graphene film as low friction solid lubricant in macroscale contact. *ACS Appl Mater Interfaces* **9**(25): 21554–21562 (2017)

[152] Liu S W, Wang H P, Xu Q, Ma T B, Yu G, Zhang C, Geng D, Yu Z, Zhang S, Wang W, et al. Robust microscale superlubricity under high contact pressure enabled by graphene-coated microsphere. *Nat Commun* **8**: 14029 (2017)

[153] Wang W, Xie G X, Luo J B. Black phosphorus as a new lubricant. *Friction* **6**(1): 116–142 (2018)

[154] Huang Y, Qiao J S, He K, Bliznakov S, Sutter E, Chen X J, Luo D, Meng F K, Su D, Decker J, et al. Interaction of black phosphorus with oxygen and water. *Chem Mater* **28**(22): 8330–8339 (2016)

[155] Ren X Y, Yang X, Xie G X, Luo J B. Black phosphorus quantum dots in aqueous ethylene glycol for macroscale superlubricity. *ACS Appl Nano Mater* **3**(5): 4799–4809 (2020)

[156] Ren X Y, Yang X, Xie G X, He F, Wang R, Zhang C H, Guo D, Luo J B. Superlubricity under ultrahigh contact pressure enabled by partially oxidized black phosphorus nanosheets. *npj 2D Mater Appl* **5**: 44 (2021)

[157] Tang G B, Wu Z B, Su F H, Wang H D, Xu X, Li Q, Ma G Z, Chu P K. Macroscale superlubricity on engineering steel in the presence of black phosphorus. *Nano Lett* **21**(12): 5308–5315 (2021)

[158] Li H, Wang J H, Gao S, Chen Q, Peng L M, Liu K H, Wei X L. 2D materials: Superlubricity between MoS_2 monolayers. *Adv Mater* **29**(27): 1701474 (2017)

[159] Zhang R F, Ning Z Y, Zhang Y Y, Zheng Q S, Chen Q, Xie H H, Zhang Q, Qian W Z, Wei F. Superlubricity in centimetres-long double-walled carbon nanotubes under ambient conditions. *Nat Nanotechnol* **8**(12): 912–916 (2013)

[160] Zhang Z, Du Y, Huang S, Meng F, Chen L, Xie W, Chang K, Zhang C, Lu Y, Lin C T, et al. Macroscale superlubricity enabled by graphene-coated surfaces. *Adv Sci* **7**(4): 1903239 (2020)

[161] Chen X C, Zhang C H, Kato T, Yang X A, Wu S D, Wang R, Nosaka M, Luo J B. Evolution of tribo-induced interfacial nanostructures governing superlubricity in a-C:H and a-C:H:Si films. *Nat Commun* **8**: 1675 (2017)

[162] Cao Z Y, Zhao W W, Liu Q, Liang A M, Zhang J Y. Super-elasticity and ultralow friction of hydrogenated fullerene-like carbon films: Associated with the size of graphene sheets. *Adv Mater Interfaces* **5**(6): 1701303 (2018)

[163] Chen X C, Li J J. Superlubricity of carbon nanostructures. *Carbon* **158**: 1–23 (2020)

[164] Spikes H A, Olver A V. Basics of mixed lubrication. *Lubr Sci* **16**(1): 1–28 (2003)

[165] Zhu Y X, Granick S. Superlubricity: a paradox about confined fluids resolved. *Phys Rev Lett* **93**(9): 096101 (2004)

[166] Feiler A A, Bergström L, Rutland M W. Superlubricity using repulsive van der Waals forces. *Langmuir* **24**(6): 2274–2276 (2008)

[167] Smith A M, Hallett J E, Perkin S. Solidification and superlubricity with molecular alkane films. *PNAS* **116**(51): 25418–25423 (2019)

[168] Trunfio-Sfarghiu A M, Berthier Y, Meurisse M H, Rieu J P. Role of nanomechanical properties in the tribological performance of phospholipid biomimetic surfaces. *Langmuir* **24**(16): 8765–8771 (2008)

[169] Zhang C X, Liu Y H, Wen S Z, Wang S. Poly(vinylphosphonic acid) (PVPA) on titanium alloy acting as effective cartilage-like superlubricity coatings. *ACS Appl Mater Interfaces* **6**(20): 17571–17578 (2014)

[170] Zhang C X, Liu Y H, Liu Z F, Zhang H Y, Cheng Q, Yang C B. Regulation mechanism of salt ions for superlubricity of hydrophilic polymer cross-linked networks on Ti_6Al_4V. *Langmuir* **33**(9): 2133–2140 (2017)

[171] Wang H D, Liu Y H, Li J J, Luo J B. Investigation of superlubricity achieved by polyalkylene glycol aqueous solutions. *Adv Mater Interfaces* **3**(19): 1600531 (2016)

[172] Liu W R, Wang H D, Liu Y H, Li J J, Erdemir A, Luo J B. Mechanism of superlubricity conversion with polyalkylene glycol aqueous solutions. *Langmuir* **35**(36): 11784–11790 (2019)

[173] Wei Q, Liu X, Yue Q, Ma S, Zhou F. Mussel-inspired one-step fabrication of ultralow-friction coatings on diverse biomaterial surfaces. *Langmuir* **35**(24): 8068–8075 (2019)

[174] Schreiber P J, Schneider J. Liquid superlubricity obtained for self-mated silicon carbide in nonaqueous low-viscosity fluid. *Tribol Int* **134**: 7–14 (2019)

[175] Jabbarzadeh A, Harrowell P, Tanner R I. Very low friction state of a dodecane film confined between mica surfaces. *Phys Rev Lett* **94**(12): 126103 (2005)

[176] Zhang C H. *Hydration force.* In *Encyclopedia of Tribology*. Boston (USA): Springer, 1704–1708, 2013.

[177] Luo J B, Wen S Z, Huang P. Thin film lubrication. Part I. Study on the transition between EHL and thin film lubrication using a relative optical interference intensity technique. *Wear* **194**(1–2): 107–115 (1996)

[178] Ma L R, Luo J B. Thin film lubrication in the past 20 years. *Friction* **4**(4): 280–302 (2016)

[179] Amann T, Kailer A. Ultralow friction of mesogenic fluid mixtures in tribological reciprocating systems. *Tribol Lett* **37**(2): 343–352 (2010)

[180] Zeng Q F. Superlubricity of NiTi alloys. In *Superlubricity*. 2nd edn. Erdemir A, Martin J M, Luo J B, Eds. Amsterdam (the Netherlands): Elsevier B.V., 2021: 517–533.

[181] Jahn S, Seror J, Klein J. Lubrication of articular cartilage. *Annu Rev Biomed Eng* **18**: 235–258 (2016)

[182] Mattei L, Puccio F D, Piccigallo B, Ciulli E. Lubrication and wear modelling of artificial hip joints: A review. *Tribol Int* **44**(5): 532–549 (2011)

[183] Höglund E. Influence of lubricant properties on elastohydrodynamic lubrication. *Wear* **232**(2): 176–184 (1999)

[184] Long Y, de Barros Bouchet M I, Lubrecht T, Onodera T, Martin J M. Superlubricity of glycerol by self-sustained chemical polishing. *Sci Rep* **9**: 6286 (2019)

[185] Uflyand I E, Zhinzhilo V A, Burlakova V E. Metal-containing nanomaterials as lubricant additives: State-of-the-art and future development. *Friction* **7**(2): 93–116 (2019)

[186] Spikes H A. Mixed lubrication—An overview. *Lubr Sci* **9**(3): 221–253 (1997)

[187] Luo J B, Zhou X. Superlubricitive engineering—Future industry nearly getting rid of wear and frictional energy consumption. *Friction* **8**(4): 643–665 (2020)

[188] Martin J M, Erdemir A. Superlubricity: Friction's vanishing act. *Phys Today* **71**(4): 40–46 (2018)

Chenhui ZHANG. He received his Ph.D. degree in mechanical engineering from Tsinghua University, China, in 2004. Then he has been working at the State Key Laboratoty of Tribology at Tsinghua University. From February 2011 to August 2011, he was invited to Luleå University of Technology in Sweden as a visiting scholar. Then he was invited to Weizmann Institute of Science in Israel as a visiting scientist from February 2012 to January 2013. His current position is a professor at Tsinghua University. His research areas cover surface coatings technology and lubrication theory. His current research interest focuses on the superlubricity.

Tianyi HAN. He received his B.S. degree in mechanical engineering from Xi'an Jiaotong University, China, in 2016, and his Ph.D. degree in mechanical engineering from Tsinghua University, China, in 2021. He is currently a post-doctor in the State Key Laboratory of Tribology at Tsinghua University. His research interests include liquid superlubricity and hydration lubrication.